Scalable Cooperative Maneuvering Using Conflict Analysis: Merging in Mixed Traffic

Hao M. Wang, Sergei S. Avedisov, *Member, IEEE*, Onur Altintas, and Gábor Orosz, *Senior Member, IEEE*

***Abstract*—This paper discusses scalable cooperative maneuvering using conflict analysis, where conflicts are managed between multiple vehicles in mixed-autonomy environments. Two different classes of cooperation, enabled by vehicle-to-everything (V2X) communication, are considered–status sharing and intent sharing. In status sharing, connected vehicles share their current states, such as position and velocity, while in intent sharing the information about vehicles' future trajectories is exchanged. The scalability of conflict analysis is studied through traffic scenarios where an ego vehicle interacts with multiple remote vehicles in a safety- and time-critical manner. We show that *pairwise* conflict analysis, which decomposes a large-scale conflict management problem to multiple sequentially solvable smaller-scale problems, is a key component of scalability. Conflict analysis, while being scaled up to more complex traffic scenarios, preserves the efficient consideration of different types of V2X information, time delay effects, and flexible control design. These results are demonstrated using simulations with real traffic data.**

***Index Terms*—V2X communication, connected and automated vehicles, conflict analysis.**

I. Introduction

TRAFFIC conflicts occur when road participants' spatiotemporal trajectories come close and trigger evasive actions [1]. Without proper management, conflicts may lead to accidents and disrupted traffic flows, jeopardizing the safety and efficiency of road transportation [2]. Recent progress in connected and automated vehicles (CAVs) [3], [4], [5], enabled by perception [6], [7], [8] and vehicle-to-everything (V2X) communication [9], [10], [11], has unlocked the potential of cooperative maneuvering, where road users cooperatively resolve conflicts [12]. The society of automotive engineers (SAE) categorizes four classes of cooperation, from low to high levels–status sharing, intent sharing, agreement seeking, and prescriptive cooperation [13]. In status sharing, connected vehicles exchange their current state (e.g., position and velocity), while in intent sharing, information about planned future motion (e.g., kinematic bounds over a future time horizon) are shared. Agreement seeking further allows vehicles to request future road space and to respond to such requests. Finally, prescriptive cooperation entails all road users following prescribed maneuvers from a coordinator.

For agreement seeking and prescriptive cooperation all participating vehicles must be highly automated (at least SAE level 3) [13]. This allows a wide range of scheduling and control strategies to be applied for conflict resolution, e.g., assume-guarantee contracts [14], graph-based modeling [15], optimal control [16], and learning-based techniques [17]. However, fully automated traffic will not come immediately. Instead, the coming decades shall witness a transition dominated by mixed traffic, where vehicles of different automation and communication capabilities coexist [18]. In this case, cooperation may be restricted to the lower two classes: status sharing and intent sharing.

Resolving conflicts in mixed traffic under lower-level cooperation involves challenges such as uncertain human-machine interaction, lack of schedule/control authority over remote agents, and limited V2X information. These issues become more prominent at scale, where a large number of participants are involved and multiple spatial and temporal constraints exist for carrying out desired maneuvers. This paper focuses on these challenges and provides new insights towards scalable cooperative maneuvering among multiple vehicles.

A. Related Work

Recent research has devoted increasing effort to study conflicts in mixed autonomy scenarios. For example, Hamilton-Jacobi (HJ) reachability analysis is a popular tool for safe control design under assumptions on environment behaviors [19]. Alternatively, correct-by-construction design of automated driving can be achieved with formal methods such as automata-based control synthesis [20]. Other approaches include multi-level optimization [21] and reinforcement learning (RL) [22], with applications in lane changes, intersections, merges, etc. In these approaches, the behaviors of uncontrolled agents are often estimated by heuristic or statistical models [23] and game theory [24].

Despite these efforts, the "curse of dimensionality" hinders the scalability of many existing approaches, where computational cost increases exponentially as the number of vehicles and maneuver constraints increases, e.g., in formal verification,

Received 16 September 2025; revised 17 January 2026; accepted 2 February 2026. Date of publication 12 February 2026; date of current version 1 July 2026. This work was supported by Toyota Motor North America Research and Development-InfoTech Labs, Mountain View, CA, USA. The Associate Editor for this article was Y. Wiseman. *(Corresponding author: Hao M. Wang.)*

Hao M. Wang is with the Department of Mechanical Engineering, University of Michigan, Ann Arbor, MI 48109 USA (e-mail: haowangm@umich.edu).

Sergei S. Avedisov and Onur Altintas are with Toyota Motor North America Research and Development, InfoTech Laboratories, Mountain View, CA 94043 USA (e-mail: sergei.avedisov@toyota.com; onur.altintas@toyota.com).

Gábor Orosz is with the Department of Mechanical Engineering and the Department of Civil and Environmental Engineering, University of Michigan, Ann Arbor, MI 48109 USA (e-mail: orosz@umich.edu).

Digital Object Identifier 10.1109/TITS.2026.3661951

1558-0016 © 2026 IEEE. All rights reserved, including rights for text and data mining, and training of artificial intelligence and similar technologies. Personal use is permitted, but republication/redistribution requires IEEE permission.
See https://www.ieee.org/publications/rights/index.html for more information.

dynamic optimization, and reachability analysis [25], [26]. Real-time implementability has thus been impaired. RL–based approaches face similar scalability challenges [27]. The joint state–action space grows combinatorially with the number of vehicles, causing high sample complexity and limited practical applicability. Hierarchical, multi-agent, or model-based strategies can partially mitigate these issues, but computational efficiency and real-time performance remain challenging [28]. A few studies have explored methods that can improve scalability in these technical tools. For example, [29] derived conditions to decouple linear systems to subsystems with separable controlled invariant sets and modular control design. In [30], multi-agent control barrier functions (CBFs) were explored to ensure safety in the presence of adversarial agents and sampled data. From the perspective of HJ reachability analysis, [31] proposed a system decomposition method for a class of nonlinear systems where backward reachable sets of the original high-dimension system can be synthesized efficiently using those of the lower-dimension subsystems.

However, a clear gap still exists in the literature when scalability of conflict management encounters V2X-enabled cooperation in mixed traffic. To our best knowledge, no previous work studied methodological scalability when connected vehicles exchange different types of V2X information under time delays. A systematic framework is absent. Real-time algorithms that account for these communication issues are also missing, and the corresponding applications in specific traffic scenarios have not been demonstrated. This paper marks an initial step to bridge this gap.

B. Contributions of This Paper

We extend the conflict analysis framework proposed in our previous work [32], [33], [34], to resolve mixed-traffic conflicts at larger scales, both in terms of the number of vehicles involved and the complexity of maneuver constraints. Conflict analysis interprets dynamical information embedded in V2X messages by constructing conflict charts. These charts divide the state space into qualitatively different domains with respect to conflict prevention. In [32], [33], and [34], conflict analysis was limited to small scale under loosely constrained spatiotemporal settings (e.g., a lane change on an infinitely long road).

In this paper we extract the essence of scalability in conflict analysis by generalizing this framework to scenarios with more vehicles and additional maneuver constraints. A highway merge is one such example, where conflicts among multiple vehicles must be resolved within a designated space and/or time domain. As shown in Fig. 1(a)-(b), a merge may be considered as a lane change that must occur within a given road section, called the merge zone, before the merging vehicle runs out of space on the on-ramp. Realizing a conflict-free merge in the presence of more surrounding vehicles, is indeed more challenging than the pure lane change considered in [34]. Note that, conflict analysis itself is not scenario-specific and it has been experimentally demonstrated using production vehicles both in merges and left/right turns [33], [35], [36].

We show that conflict analysis is scalable and the number of vehicles and the number of constraints increase. A key

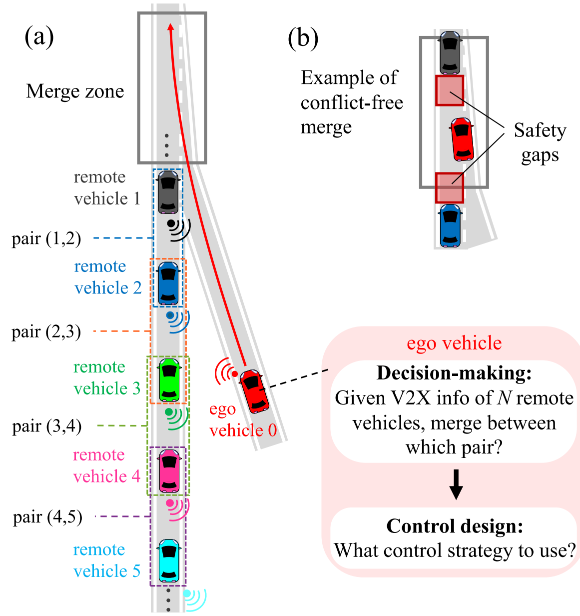

Fig. 1. (a) A merge scenario involving an ego vehicle 0 and N remote vehicles, where the example of $N = 5$ is shown. Remote vehicle pairs are highlighted. The ego vehicle needs to make decisions on its maneuver and design corresponding control strategies. (b) An example of a conflict-free merge maneuver where the ego vehicle, while inside the designated merge zone, forms necessary front and rear safety gaps with a pair of remote vehicles.

component of scalability is *pairwise* conflict analysis, which decomposes a large-scale conflict management problem to multiple sequentially solvable smaller-scale problems. Our approach projects the reachable tubes onto lower dimensional subspaces and decouples the environment uncertainties and the ego vehicle's behavior capabilities. These techniques enable real-time implementable decision-making algorithms that are efficient for managing larger-scale traffic conflicts.

We study the scalability of conflict analysis under the aforementioned two classes of cooperation for mixed traffic: status sharing and intent sharing. Moreover, we consider two types of time delays, one in V2X communication and the other in vehicle dynamics. Throughout our analysis, we show that the generalized conflict analysis framework allows efficient decision-making and flexible control design. The conflict analysis framework incorporates different V2X information and delay effects. These results are demonstrated using simulations based on real traffic data.

The major contributions of this paper are threefold. (i) We generalize conflict analysis to a larger scale which accommodates more vehicles under stricter maneuver constraints. (ii) We investigate the methodological scalability of mixed-traffic conflict management subject to status-sharing and intent-sharing cooperation and delay effects. (iii) Real-time decision-making and control algorithms are developed and validated through real traffic data.

The remainder of this paper is structured as follows. In Section II we model vehicle dynamics and the communications between vehicles. We then propose *pairwise* conflict analysis in Section III. In Section IV we extract the essence of scalability in our reachability-based approach from a lane change

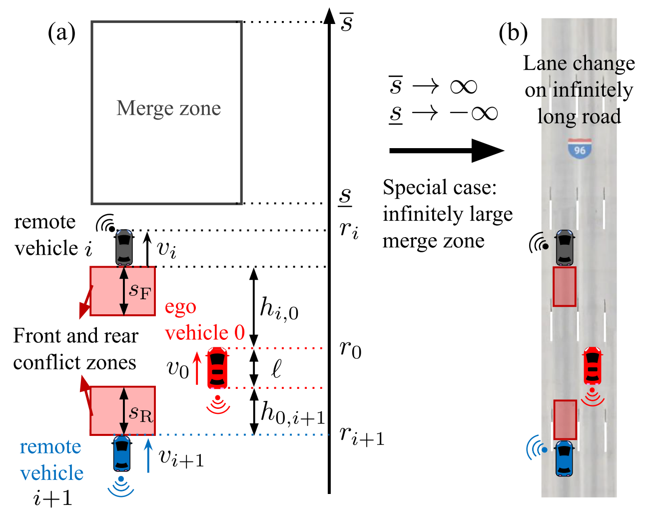

Fig. 2. (a) Generalized model of the merge scenario, where the ego vehicle 0 and remote vehicles i and $i+1$ are shown. (b) A special case where the merge zone becomes infinitely large. This corresponds to a lane change maneuver on an infinitely long road.

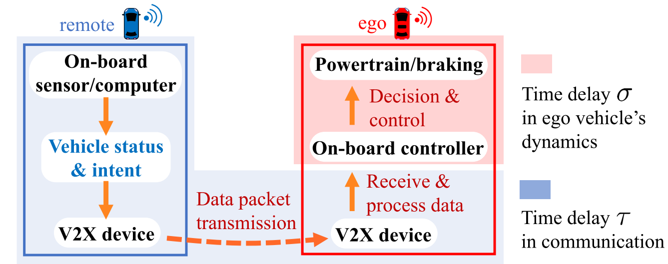

Fig. 3. Time delays considered in this paper, including communication and actuation delays.

TABLE I
PARAMETERS VALUES USED IN THIS PAPER ($i = 1, \ldots, N$)

s_F, s_R	10 [m]	l	5 [m]
$a_{\min,0}$	-8 [m/s^2]	$a_{\min,i}$	-4 [m/s^2]
$a_{\max,0}$	4 [m/s^2]	$a_{\max,i}$	2 [m/s^2]
$v_{\min,0}$	17 [m/s]	$v_{\min,i}$	20 [m/s]
$v_{\max,0}$	33 [m/s]	$v_{\max,i}$	30 [m/s]

scenario and generalize it to accommodate stricter maneuver constraints. In Section V, controllers are designed and real highway data is used for validation. Section VI concludes the paper and discusses future directions.

II. MODELING VEHICLE DYNAMICS AND COMMUNICATION

This section introduces the vehicle dynamics models and the V2X communication setup that will be used throughout this paper. To study the scalability of conflict management in mixed traffic, we consider a multi-vehicle merge scenario depicted in Fig. 1(a) where an ego vehicle 0 seeks to merge onto the main road as a chain of N remote vehicles, indexed $1, \ldots, N$, are approaching along that road. To perform a conflict-free merge, the ego vehicle must select an appropriate target pair of remote vehicles to merge between and then perform the following two steps: (i) stay on the ramp and create adequate longitudinal distances from the two remote vehicles while inside a designated merge zone; (ii) move into the main road by changing its lateral position. A conflict-free merge example is visualized in Fig. 1(b). In this paper, we focus on step (i) and assume that step (ii) is carried out by lateral motion planners and controllers once the longitudinal distances are ensured within the merge zone.

The merge zone is defined towards the end of the ramp with a finite length, occupying the position domain $[\underline{s}, \overline{s}]$; see the generalized model in Fig. 2(a) where the remote vehicles i and $i+1$ are shown. For simplicity, the necessary front and rear safety distances to ensure a conflict-free merge are represented by two conflict zones of constant lengths s_F and s_R. These conflict zones move together with the corresponding remote vehicles. Without loss of generality, we use the same values of s_F and s_R for all vehicles. Our analysis can be generalized to speed-dependent, non-constant sizes of conflict zones.

To reduce the computational complexity of conflict analysis we focus on the longitudinal dynamics of the vehicles. Prior experimental works have validated conflict analysis for merges [36], [37], and right turns [35] using a real experimental vehicle, showing that considering longitudinal dynamics is sufficient.

We describe the vehicles' longitudinal dynamics below, with the aerodynamic drag and rolling resistance neglected:

$$\begin{aligned} \dot{r}_0(t) &= v_0(t), & \dot{v}_0(t) &= \mathrm{sat}(u_0(t-\sigma)), \\ \dot{r}_i(t) &= v_i(t), & \dot{v}_i(t) &= \mathrm{sat}(u_i(t)), \qquad i = 1, \ldots, N, \end{aligned} \tag{1}$$

where r_0 and r_i are the vehicle's front bumper positions, v_0 and v_i are longitudinal velocities, the dot denotes the derivative with respect to time t, u_0 and u_i are the control inputs. For the ego vehicle, we include an input delay σ to model the time delays existing in its powertrain/braking systems and in its on-board controllers; see Fig. 3. For the remote vehicles, however, we do not explicitly consider such delays. This represents our limited knowledge about their dynamics. Note that, as will be discussed later, the lack of such knowledge is compensated by the intent information transmitted from the remote vehicles. The limits of acceleration are modeled by the saturation function sat(·). For $v \in (v_{\min}, v_{\max})$, one has

$$\mathrm{sat}(u) = \max\left\{\min\{u, a_{\max}\}, a_{\min}\right\}. \tag{2}$$

For $v = v_{\min}$, one shall substitute $a_{\min}$ with 0, because the vehicle does not decelerate below the minimum speed; for $v = v_{\max}$, one shall substitute $a_{\max}$ with 0, since the vehicle does not accelerate above the maximum speed. We remark that the values of acceleration and velocity limits depend on the road conditions and driving scenarios. Here we use limits corresponding to the typical driving behaviors on highways, with the assumption that the ego vehicle has the knowledge about these values; see Table I. We define the system state of model (1) as

$$\mathbf{X} := [r_0, v_0, r_1, v_1, \ldots, r_N, v_N]^\top \in \Omega, \tag{3}$$

where Ω is a $2(N+1)$-dimensional state space given as

$$\Omega: = [-\infty, \overline{s}] \times [v_{\min,0}, v_{\max,0}] \times [-\infty, \overline{s}] \times [v_{\min,1}, v_{\max,1}]$$

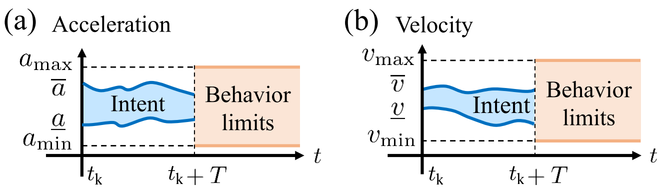

Fig. 4. A conceptual illustration of intent information (without communication delay).

$$\times \cdots \times [-\infty, \overline{s}] \times [v_{\min,N}, v_{\max,N}] \tag{4}$$

The indicated position domains suggest that our analysis considers the merge scenario until the corresponding vehicles exit the merge zone.

We resolve conflicts from the perspective of the ego vehicle. Again, remote vehicles are assumed to be outside our control, but the ego vehicle has the knowledge about their velocity and acceleration limits corresponding to typical highway driving; see Table I. In addition, all vehicles are assumed to be capable of V2X communication. Since the remote vehicles may be subject to different automation levels, only lower-level cooperation may be feasible between the ego and remote vehicles. We consider that the V2X information that the ego vehicle receives from the remote vehicles is restricted to two types: status and intent. The status information of a remote vehicle i contains its instantaneous position r_i and velocity v_i, while the intent information encodes a restricted domain of velocity and acceleration over a future time horizon of finite length T_i:

$$v_i(t) \in [\underline{v}_i(t), \overline{v}_i(t)], \quad u_i(t) \in [\underline{a}_i(t), \overline{a}_i(t)]. \tag{5}$$

A visualization of such intent is highlighted in blue in Fig. 4. Note that while status information has been well-standardized (e.g., basic safety messages (BSMs)), different representations of vehicle motion intent exist in the literature [38], [39], [40], [41]. Our representation of intent follows the one used in our previous work [33], which is suitable for describing a merge maneuver while focusing on the longitudinal motion. The velocity and acceleration ranges are capable of encoding motion uncertainty, and can thus describe intent of vehicles at different automation levels. For instance, a human-driven vehicle's intent may be generated in a data-driven manner from the diver's historical behaviors, while an automated vehicle may synthesize such intent from its motion planner.

To focus on studying the methodological scalability of conflict management, we adopt a simplification by considering synchronized status and intent reception from all remote vehicles. That is, the ego vehicle receives updated status and intent messages at each discrete times t_k, $k = 0, 1, \ldots$, from all remote vehicles, where t_0 is the first time the ego vehicle receives V2X information in the maneuver. Note that our analysis can be naturally extended to accommodate asynchronous status and intent transmission. Our previous work [33] gives details of handling unsynchronized communication in conflict resolution. To accommodate imperfect communication, we consider the information delay τ_i associated with each remote vehicle i. Thus, at each time t_k, the ego vehicle receives status information encoding $[r_i(t_k-\tau_i), v_i(t_k-\tau_i)]$ for all $i \in \{1, \ldots, N\}$ and intent information encoding the velocity and acceleration range (5) over the time horizon

$$t \in [t_k - \tau_i, \max\{t_k, t_k + T_i - \tau_i\}], \tag{6}$$

for all $i \in \{1, \ldots, N\}$. The horizon (6) gives the time range during which intent information remains valid under the communication delay τ_i. If the delayed duration is longer than the intent horizon itself, i.e., $\tau_i \geq T_i$, then the intent is expired by the time the ego vehicle receives it. We remark again that different remote vehicles may be subject to different transmission delays τ_i, but it is assumed that the ego vehicle's V2X port receives status and intent information synchronously from all remote vehicles. Note that τ_i may take different values at each time t_k. Such time-varying delays are accommodated within our framework.

With the mathematical models and communication settings presented above, we are now ready to perform conflict analysis.

III. Pairwise Conflict Analysis

In this section, we establish the notion of pairwise conflict analysis, which constitutes a key component of scalability in multi-vehicle conflict management. We start by formalizing the conflict-free maneuver using formal logic.

Recall that to prevent a conflict, the ego vehicle must first determine a target pair of remote vehicles, and then secure the required safety distances inside a designated merge zone before changing lanes. Given remote vehicles $1, \ldots, N$, at a time t_k (when the ego vehicle receives V2X information), a conflict-free maneuver can be mathematically expressed by the proposition

$$\begin{aligned} M := \{&\exists t \geq t_k, \exists i \in \{1, \ldots, N-1\}, \\ &h_{i,0}(t) \geq s_{\mathrm{F}} \wedge h_{0,i+1}(t) \geq s_{\mathrm{R}} \wedge r_0(t) \in [\underline{s}, \overline{s}]\}. \end{aligned} \tag{7}$$

Here, the symbol $\wedge$ is logical conjunction "and", while

$$h_{i,0} := r_i - r_0 - \ell, \quad h_{0,i+1} := r_0 - r_{i+1} - \ell, \tag{8}$$

give the front and rear gaps between the ego vehicle 0 and the remote vehicles i and $i+1$; see illustration in Fig. 2(a). Note that these are signed bumper-to-bumper distances, and for simplicity, all vehicles are assumed to have the length ℓ.

Proposition M can be further decomposed into three cases:

(i) No-conflict case: ego vehicle 0 is able to prevent conflict independent of the motion of remote vehicles $1, \ldots, N$.
(ii) Uncertain case: ego vehicle 0 may be able to prevent conflict depending on the motion of remote vehicles $1, \ldots, N$.
(iii) Conflict case: ego vehicle 0 is not able to prevent conflict independent of the motion of remote vehicles $1, \ldots, N$.

These cases correspond to three pairwise disjoint sets in the state space Ω of system (1), defined as

$$\mathcal{M}_{\mathrm{g}} := \{\mathbf{X}(t_k) \in \Omega | \forall u_1(t), \ldots, \forall u_N(t), \exists u_0(t), M\}, \tag{9}$$

$$\begin{aligned} \mathcal{M}_{\mathrm{y}} := \{&\mathbf{X}(t_k) \in \Omega | (\exists u_1(t), \ldots, \exists u_N(t), \forall u_0(t), \neg M) \wedge \\ &(\exists u_1(t), \ldots, \exists u_N(t), \exists u_0(t), M)\}, \end{aligned} \tag{10}$$

$$\mathcal{M}_{\mathrm{r}} := \{\mathbf{X}(t_k) \in \Omega | \forall u_1(t), \ldots, \forall u_N(t), \forall u_0(t), \neg M\}, \tag{11}$$

where the symbol $\neg$ means negation, and $u_0(t), \ldots, u_N(t)$ are functions of time $t \geq t_k$. These sets are referred to as no-conflict set, uncertain set, and conflict set, respectively. In this paper, we use green, yellow, and red colors to visualize these domains, and accordingly, the subscripts "g", "y", and "r" are used. Note that the definition (10) contains two predicates that negate those of (9) and (11), i.e.,

$$(\exists u_1, \ldots, u_N, \forall u_0, \neg M) \Longleftrightarrow \neg(\forall u_1, \ldots, u_N, \exists u_0, M), \quad (12)$$

$$(\exists u_1, \ldots, u_N, \exists u_0, M) \Longleftrightarrow \neg(\forall u_1, \ldots, u_N, \forall u_0, \neg M). \quad (13)$$

Thus, the sets $\mathcal{M}_{\mathrm{g}}$, $\mathcal{M}_{\mathrm{y}}$, and $\mathcal{M}_{\mathrm{r}}$ are indeed pairwise disjoint, and $\mathcal{M}_{\mathrm{g}} \cup \mathcal{M}_{\mathrm{y}} \cup \mathcal{M}_{\mathrm{r}} = \Omega$.

Given the available V2X information, identifying the set to which the current system state $\mathbf{X}$ belongs is an important step towards conflict management, as it informs the ego vehicle of the feasibility to accomplish the maneuver and provides insights for controller design. For instance, definition (9) indicates that a conflict-free control strategy is guaranteed if $\mathbf{X} \in \mathcal{M}_{\mathrm{g}}$. Reachability-based approaches are often used to calculate these sets, check the system state's set membership, and derive corresponding control laws. Techniques include solving HJ partial differential equations [19] and polytope-based set approximations [42]. Recall that the state space Ω has a dimension of $2(N+1)$. As the system scales and N becomes large, dimensionality challenges arise with the existing methods. To tackle this issue, below we develop pairwise conflict analysis, which aims to reason about large-scale conflict prevention through a sequence of smaller-scale conflict management problems.

Consider the local conflict between the ego vehicle 0 and a pre-determined target pair of remote vehicles i and $i+1$; see Fig. 2(a). The corresponding conflict-free merge condition can be described by the proposition

$$M_i := \{\exists t \geq t_k,\ h_{i,0}(t) \geq s_{\mathrm{F}} \wedge h_{0,i+1}(t) \geq s_{\mathrm{R}} \wedge r_0(t) \in [\underline{s}, \overline{s}]\}. \quad (14)$$

Given the dynamics (1), we define a local state variable

$$\mathbf{x}_i := [h_{i,0}, h_{0,i+1}, r_0, v_0, v_i, v_{i+1}]^\top \in \Omega_i, \quad (15)$$

where Ω_i is a 6-dimensional state space given as

$$\Omega_i := \{[h_{i,0}, h_{0,i+1}]^\top \in \mathbb{R}^2 | h_{i,0} + h_{0,i+1} \geq -l\} \times (-\infty, \overline{s}] \times [v_{\min,0}, v_{\max,0}] \times [v_{\min,i}, v_{\max,i}] \times [v_{\min,i+1}, v_{\max,i+1}], \quad (16)$$

cf. (3) and (4). Noting that the total distance between vehicles i and $i+1$ is given by

$$h_{i,i+1} := h_{i,0} + h_{0,i+1} + \ell, \quad (17)$$

the condition $h_{i,0} + h_{0,i+1} \geq -\ell$ in (16) guarantees that the vehicle $i+1$ always follows vehicle i without a collision. Analogous to (9)-(11), Ω_i can be partitioned into the no-conflict, uncertain, and conflict sets as

$$\mathcal{M}_{\mathrm{g}}^i := \{\mathbf{x}_i(t_k) \in \Omega_i | \quad \forall u_i(t), \forall u_{i+1}(t), \exists u_0(t), M_i\}, \quad (18)$$

$$\mathcal{M}_{\mathrm{y}}^i := \{\mathbf{x}_i(t_k) \in \Omega_i | (\exists u_i(t), \exists u_{i+1}(t), \quad \forall u_0(t), \neg M_i) \wedge (\exists u_i(t), \exists u_{i+1}(t), \exists u_0(t), M_i)\}, \quad (19)$$

$$\mathcal{M}_{\mathrm{r}}^i := \{\mathbf{x}_i(t_k) \in \Omega_i | \forall u_i(t), \forall u_{i+1}(t), \quad \forall u_0(t), \neg M_i\}. \quad (20)$$

The sets $\mathcal{M}_{\mathrm{g}}^i$, $\mathcal{M}_{\mathrm{y}}^i$, and $\mathcal{M}_{\mathrm{r}}^i$ in local conflict management have much smaller dimensions, compared to the sets $\mathcal{M}_{\mathrm{g}}$, $\mathcal{M}_{\mathrm{y}}$, and $\mathcal{M}_{\mathrm{r}}$, which allows for tractable set calculation and/or set membership check. We present the following Theorem to show that such dimensionality advantages can be exploited to infer larger-scale conflicts from smaller-scale ones.

Theorem 1: Given the dynamics (1)-(2), the current system state $\mathbf{X}(t_k) \in \Omega$, and current local states $\mathbf{x}_i(t_k) \in \Omega_i$, $i \in \{1, \ldots, N-1\}$, the following two relationships hold:

$$\mathbf{X}(t_k) \in \mathcal{M}_{\mathrm{g}} \Longleftrightarrow \exists i \in \{1, \ldots, N-1\}, \mathbf{x}_i(t_k) \in \mathcal{M}_{\mathrm{g}}^i, \quad (21)$$

$$\mathbf{X}(t_k) \in \mathcal{M}_{\mathrm{r}} \Longleftrightarrow \forall i \in \{1, \ldots, N-1\}, \mathbf{x}_i(t_k) \in \mathcal{M}_{\mathrm{r}}^i. \quad (22)$$

Proof: See Appendix A. □

The relationships (21) and (22) justify that the conflicts with all N remote vehicles can be reasoned about using adjacent remote vehicle pairs, each pair i consisting of vehicles i and $i+1$. In particular, the right hand side of (21) indicates that finding such an i would suffice the global conflict prevention purpose. One feasible approach to finding such an i is by checking $\mathbf{x}_i(t_k) \in \mathcal{M}_{\mathrm{g}}^i$ sequentially for each $i \in \{1, \ldots, N-1\}$. Computation-wise, as will be shown later, algorithms with bounded linear time complexity exist for checking such local conflicts. Thus, sequential check is efficiently implementable in real-time. Note that one may follow different orders to search for a desired remote vehicle pair. However, the proposed sequential check ensures that the earliest found solution yields the best travel time efficiency, in the sense that the ego vehicle can achieve a further ahead position once the merge maneuver is completed.

We remark that depending on traffic scenarios, pairwise conflict analysis can be extended such that each "pair" of remote vehicles consists of more than two vehicles. Indeed, the key to pairwise conflict analysis is to identify remote vehicle groups of the smallest possible size, such that resolving local conflicts in lower dimension leads to global conflict resolution. Here, we use the multi-vehicle merge scenario as an example to provide insights on pairwise conflict analysis. Finding a general solution that is applicable to all traffic scenarios is beyond the scope of this paper and remains a future tasks.

With these, we now explore the methodological scalability of checking local conflicts that involve the ego vehicle 0 and remote vehicles i and $i+1$.

IV. Scalable Local Conflict Analysis

In this section, we develop methods to study local conflicts. That is, we check whether a given local state $\mathbf{x}_i(t_k)$ is located in the set $\mathcal{M}_{\mathrm{g}}^i$, $\mathcal{M}_{\mathrm{y}}^i$, or $\mathcal{M}_{\mathrm{r}}^i$. We extract the essence of scalability in our methods, which allows for real-time implementation. Our discussion starts with the simpler case where the communication delays are ignored, i.e., $\tau_i = 0$ for each remote vehicle i. We then extend our theory to accommodate non-zero communication delays in subsection IV-B.

Without communication delays, the current system state $\mathbf{x}_i(t_k)$ is available to the ego vehicle. We first notice that if $h_{i,0}(t_k) \geq s_{\mathrm{F}} \wedge h_{0,i+1}(t_k) \geq s_{\mathrm{R}} \wedge r_0(t_k) \in [\underline{s}, \overline{s}]$ holds, then $\mathbf{x}_i(t_k) \in \mathcal{M}_{\mathrm{g}}^i$ holds immediately since the ego vehicle already formed necessary gaps inside the merge zone. Otherwise, one needs to check if the proposition M_i is true for some $t > t_k$, considering all possible future behaviors of the ego and remote vehicles. The following Lemma simplifies this task by justifying that using the remote vehicles' behavioral limits would suffice in checking $\mathbf{x}(t_k) \in \mathcal{M}^i_{\rm g}$.

Lemma 1: The following relationship holds for any given current local state $\mathbf{x}_i(t_k) \in \Omega_i$:

$$\begin{aligned}&\{\forall u_i(t), \forall u_{i+1}(t), \exists u_0(t), M_i\} \iff \\ &\{(u_i(t), u_{i+1}(t)) \equiv (\underline{u}_i(t), \overline{u}_{i+1}(t)), \exists u_0(t), \exists t \in [t_k, t_{\max,0}], \\ &h_{i,0}(t) \geq s_{\rm F} \wedge h_{0,i+1}(t) \geq s_{\rm R} \wedge r_0(t) \in [\underline{s}, \overline{s}]\},\end{aligned} \tag{23}$$

where

$$\underline{u}_i(t) = \begin{cases} \underline{a}_i(t), & \text{if } t \in [t_k, t_k + T_i], \\ a_{\min,i}, & \text{otherwise}, \end{cases} \tag{24}$$

$$\overline{u}_{i+1}(t) = \begin{cases} \overline{a}_{i+1}(t), & \text{if } t \in [t_k, t_k + T_{i+1}], \\ a_{\max,i+1}, & \text{otherwise}, \end{cases} \tag{25}$$

with $t_{\max,0}$ being the time t such that $r_0(t) = \overline{s}$ under the control input

$$\overline{u}_0(t) = \begin{cases} u_0(t), & \text{if } t \in [t_k - \sigma, t_k], \\ a_{\max,0}, & \text{otherwise}. \end{cases} \tag{26}$$

Proof: See Appendix B. □

Here, $\underline{u}_i(t)$ and $\overline{u}_{i+1}(t)$ are the input lower and upper bounds of the remote vehicles i and $i+1$, respectively, given the available intent information. These inputs represent the remote vehicles' worst-case behaviors that shrink the total distance between the two vehicles in the fastest manner. Also, the input $\overline{u}_0(t)$ generates the smallest position that the ego vehicle may reach, under its input limits and delay σ in its dynamics. Accordingly, $t_{\max,0}$ gives the latest possible time of the ego vehicle remaining inside the merge zone. Thus, Lemma 1 suggests that to prevent conflict independently of the remote vehicles' motion, the ego vehicle must form the necessary gaps inside the merge zone within the time window $[t_k, t_{\max,0}]$, assuming the worst-case motion of remote vehicles. This way, checking $\mathrm{x}_i(t_k) \in \mathcal{M}^i_{\rm g}$ is reduced to checking the existence of an input $u_0(t)$ for $t \geq t_k$ and a time $t \in [t_k, t_{\max,0}]$ such that $h_{i,0}(t) \geq s_{\rm F} \wedge h_{0,i+1}(t) \geq s_{\rm R} \wedge r_0(t) \in [\underline{s}, \overline{s}]$ holds under the remote vehicles' (deterministic) worst-case behaviors.

We emphasize that being able to consider deterministic behaviors of the remote vehicles allows us to bypass the environmental uncertainties from the rest of our analysis. A similar relationship can be derived for checking $\mathrm{x}_i(t_k) \in \mathcal{M}^i_{\rm r}$ as stated by the following Lemma.

Lemma 2: The following relationship holds for any given current state $\mathbf{x}_i(t_k) \in \Omega_i$:

$$\begin{aligned}&\{\forall u_i(t), \forall u_{i+1}(t), \forall u_0(t), \neg M_i\} \iff \\ &\{(u_i(t), u_{i+1}(t)) \equiv (\overline{u}_i(t), \underline{u}_{i+1}(t)), \forall u_0(t), \forall t \in [t_k, t_{\max,0}], \\ &\neg(h_{i,0}(t) \geq s_{\rm F} \wedge h_{0,i+1}(t) \geq s_{\rm R} \wedge r_0(t) \in [\underline{s}, \overline{s}])\},\end{aligned} \tag{27}$$

where

$$\overline{u}_i(t) = \begin{cases} \overline{a}_i(t), & \text{if } t \in [t_k, t_k + T_i], \\ a_{\max,i}, & \text{otherwise}, \end{cases} \tag{28}$$

$$\underline{u}_{i+1}(t) = \begin{cases} \underline{a}_{i+1}(t), & \text{if } t \in [t_k, t_k + T_{i+1}], \\ a_{\min,i+1}, & \text{otherwise}, \end{cases} \tag{29}$$

and $t_{\max,0}$ is given in Lemma 1.

Proof: See Appendix C. □

Here, $\overline{u}_i(t)$ and $\underline{u}_{i+1}(t)$ are the upper and lower input bounds of the remote vehicles i and $i+1$, respectively. Such inputs give the remote vehicles' best-case behaviors that maximizes the total distance between the two vehicles. Lemma 2 suggests that a conflict-free merge maneuver being impossible is equivalent to the fact that the ego vehicle is not able to form the necessary gaps inside the merge zone within the time window $[t_k, t_{\max,0}]$, assuming the best-case motion of remote vehicles. That is, checking $\mathrm{x}(t_k) \in \mathcal{M}^i_{\rm r}$ is reduced to showing the inexistence of an input $u_0(t)$ for $t \geq t_k$ and a time $t \in [t_k, t_{\max,0}]$ to satisfy the condition $h_{i,0}(t) \geq s_{\rm F} \wedge h_{0,i+1}(t) \geq s_{\rm R} \wedge r_0(t) \in [\underline{s}, \overline{s}]$ under the remote vehicles' (deterministic) best-case behaviors.

With Lemmas 1 and 2, we are now ready to develop criteria for checking $\mathbf{x}_i(t_k) \in \mathcal{M}^i_{\rm g}$ and $\mathbf{x}_i(t_k) \in \mathcal{M}^i_{\rm r}$. We start with the special case $\underline{s} \to -\infty$ and $\overline{s} \to \infty$, i.e., when the merge zone is infinitely large. This reduces the original merge scenario to a lane change on a long (enough) road, where the ego vehicle's maneuver is regarded conflict-free whenever the safety gaps are formed. Note that this is the scenario studied in our previous work [34]. Such a special case still satisfies Lemmas 1 and 2 with $t_{\max,0} \to \infty$. Below we revisit the methodology used therein from a scalability perspective. We then extend our analysis to accommodate the geometrical constraints under finite $\underline{s}$ and $\overline{s}$.

A. Lane Change: Infinitely Large Merge Zone

When $\underline{s} \to -\infty$ and $\overline{s} \to \infty$, one can drop the condition $r_0(t) \in [\underline{s}, \overline{s}]$ in proposition M_i. We use $\tilde{M}_i$ to denote this special case:

$$\tilde{M}_i := \{\exists t \geq t_k,\ h_{i,0}(t) \geq s_{\rm F} \wedge h_{0,i+1}(t) \geq s_{\rm R}\}, \tag{30}$$

cf. (14). In a lane change, the absolute position of the ego vehicle 0 is no longer of interest. One can thus drop the r_0 element from the state variable $\mathbf{x}_i$ and remove the corresponding dimension from the state space Ω_i, which yields the state variable

$$\tilde{\mathbf{x}}_i := [h_{i,0}, h_{0,i+1}, v_0, v_i, v_{i+1}]^\top \in \tilde{\Omega}_i, \tag{31}$$

with a truncated 5-dimensional state space

$$\begin{aligned}\tilde{\Omega}_i :&= \{[h_{i,0}, h_{0,i+1}]^\top \in \mathbb{R}^2 | h_{i,0} + h_{0,i+1} \geq -l\} \\ &\times [v_{\min,0}, v_{\max,0}] \times [v_{\min,i}, v_{\max,i}] \\ &\times [v_{\min,i+1}, v_{\max,i+1}],\end{aligned} \tag{32}$$

cf. (15) and (16). By replacing $\mathbf{x}_i$, Ω_i, and M_i with $\tilde{\mathbf{x}}_i$, $\tilde{\Omega}_i$, and $\tilde{M}_i$, one obtains three sets partitioning the state space $\tilde{\Omega}_i$: no-conflict set $\tilde{\mathcal{M}}^i_{\rm g}$, uncertain set $\tilde{\mathcal{M}}^i_{\rm y}$, and conflict set $\tilde{\mathcal{M}}^i_{\rm r}$, analogous to (18)-(20),

An example of the sets $\tilde{\mathcal{M}}^i_{\rm g}$, $\tilde{\mathcal{M}}^i_{\rm y}$, and $\tilde{\mathcal{M}}^i_{\rm r}$ is shown in $(h_{i,0}, h_{0,i+1})$-plane in Fig. 5(a) for the velocities $(v_0, v_i, v_{i+1}) = (25, 24.5, 24.3)$ [m/s] under the delay $\sigma = 0.5$ [s] in the ego vehicle's dynamics. The domain outside the set $\tilde{\Omega}_i$ is left blank; cf. (32). Fig. 5(a) is referred to as conflict chart. From the ego vehicle's viewpoint, calculating these sets on-board

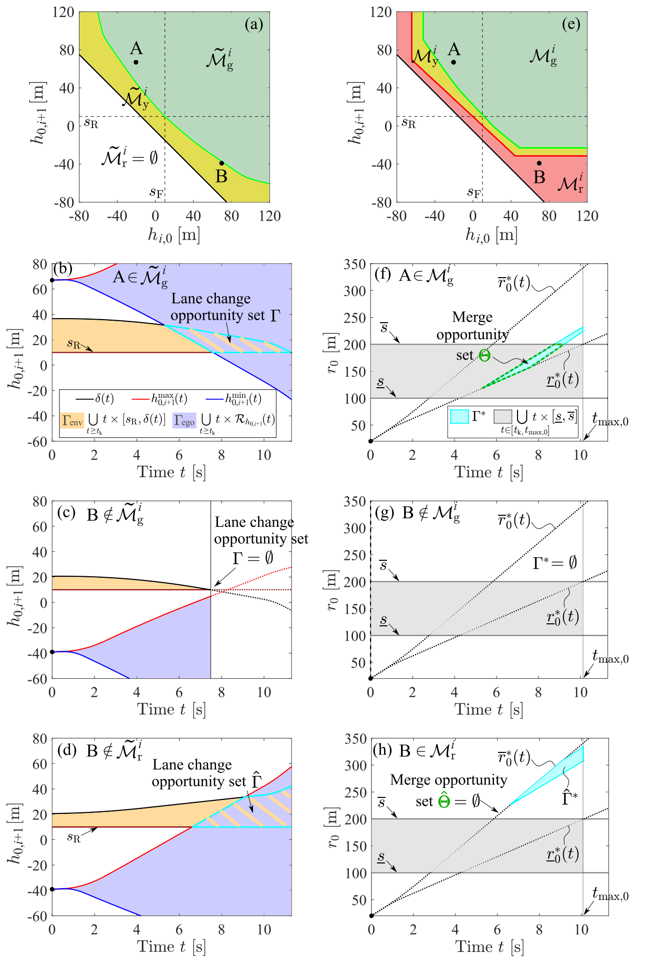

Fig. 5. (a)-(d) Conflict analysis corresponding to the special case where the merge zone is infinitely large, i.e., lane change scenario. (a) Conflict chart in the $(h_{i,0}, h_{0,i+1})$-plane at time $t_k = 0$, with the velocities $(v_0(0), v_i(0), v_{i+1}(0))$ and the state points A and B given in Table II. (b)-(d) Constructions of the lane change opportunity set Γ that indicates $\mathrm{A} \in \tilde{\mathcal{M}}_g^i$, $\mathrm{B} \notin \tilde{\mathcal{M}}_g^i$, and $\mathrm{B} \notin \tilde{\mathcal{M}}_r^i$, respectively. Time delay $\sigma = 0.5$ [s] is used in the ego vehicle's dynamics. Intent of remote vehicles are summarized in Table II. These are obtained from real highway driving data. (e)-(h) Conflict analysis corresponding to the merge scenario, where the ego vehicle 0 has initial position $r_0(0) = 20$ [m], and the merge zone is located at [100, 200] [m]. The remote vehicles' conditions remain the same as in (a)-(d). (f)-(h) show the constructions of the merge opportunity set Θ that indicates $\mathrm{A} \in \mathcal{M}_g^i$, $\mathrm{B} \notin \mathcal{M}_g^i$, and $\mathrm{B} \in \mathcal{M}_r^i$, respectively.

TABLE II
VEHICLE STATUS AND INTENT USED IN CONSTRUCTING FIG. 5

Status	Velocities: $(v_0(0), v_i(0), v_{i+1}(0)) = (25, 24.5, 24.3)$ [m/s] Point A: $(h_{i,0}(0), h_{0,i+1}(0)) = (-20.4, 66.9)$ [m] Point B: $(h_{i,0}(0), h_{0,i+1}(0)) = (69.6, -39.1)$ [m]
Intent	$v_i(t) \in [23.0, 24.8]$ [m/s], $u_i(t) \in [-0.11, 0.18]$ [m/s^2] $v_{i+1}(t) \in [24.3, 26.5]$ [m/s], $u_{i+1}(t) \in [-0.2, 0.33]$ [m/s^2] Horizon: $T_i = T_{i+1} = 10$ [s]

is not necessary. Instead, it suffices to only check which set the current system state belongs to once the latest V2X information is received. The conflict chart itself can then be synthesized by examining each state in the state space $\tilde{\Omega}_i$. The criteria for checking $\tilde{\mathbf{x}}_i(t_k) \in \tilde{\mathcal{M}}_{\mathrm{g}}^i$, $\tilde{\mathcal{M}}_{\mathrm{y}}^i$, and $\tilde{\mathcal{M}}_{\mathrm{r}}^i$ are thus our focus.

Notice that $\tilde{\mathcal{M}}_{\mathrm{r}}^i = \emptyset$ holds in this example. We remark that, as shown in [34], for any finite delay σ in the ego vehicle's dynamics, and for any feasible intent of the remote vehicles with finite time horizons, $\tilde{\mathcal{M}}_{\mathrm{r}}^i = \emptyset$ holds if the parameters of behavior limits satisfy the condition

$$(v_{\max,i} > v_{\min,i+1}) \wedge (v_{\max,0} > v_{\min,i+1}) \wedge (v_{\min,0} < v_{\max,i}), \tag{33}$$

cf. parameters in Table I. This condition enables the remote vehicles to eventually create sufficiently large distance between them (if vehicle i speeds up and vehicle $i+1$ decelerates), such that the ego vehicle can perform a conflict-free lane change. Unlike [34], our discussion below considers a more general setting where the condition (33) does not necessarily hold.

The following Theorem gives a reachability-based criterion for checking $\tilde{\mathbf{x}}_i(t_k) \in \tilde{\mathcal{M}}_{\mathrm{g}}^i$.

Theorem 2: Given the dynamics (1)-(2) and the state $\tilde{\mathbf{x}}_i(t_k) \in \tilde{\Omega}_i$, $\tilde{\mathbf{x}}_i(t_k) \in \tilde{\mathcal{M}}_{\mathrm{g}}^i$ holds if and only if the condition

$$\Gamma := \Gamma_{\mathrm{env}} \cap \Gamma_{\mathrm{ego}} \neq \emptyset, \tag{34}$$

is satisfied under $(u_i(t), u_{i+1}(t)) \equiv (\underline{u}_i(t), \overline{u}_{i+1}(t))$, where

$$\Gamma_{\mathrm{env}} = \bigcup_{t \geq t_k} t \times [s_{\mathrm{R}}, \delta(t)], \tag{35}$$

$$\Gamma_{\mathrm{ego}} = \bigcup_{t \geq t_k} t \times \mathcal{R}_{h_{0,i+1}}(t), \tag{36}$$

$\delta(t) = h_{i,i+1}(t) - s_{\mathrm{F}} - l$, and $\mathcal{R}_{h_{0,i+1}}(t) = [h_{0,i+1}^{\min}(t), h_{0,i+1}^{\max}(t)]$. Here, $h_{0,i+1}^{\min}(t)$ and $h_{0,i+1}^{\max}(t)$ are the $h_{0,i+1}(t)$ calculated under the ego vehicle's inputs

$$\underline{u}_0(t) = \begin{cases} u_0(t), & \text{if } t \in [t_k - \sigma, t_k], \\ a_{\min,0}, & \text{otherwise}, \end{cases} \tag{37}$$

and $\overline{u}_0(t)$ given in (26), respectively.

Proof: See Appendix D. □

Notice that $\delta(t)$, $h_{0,i+1}^{\min}(t)$, and $h_{0,i+1}^{\max}(t)$ are deterministic functions of time t that can be calculated by a variety of numerical integration methods. Given the total distance $h_{i,i+1}(t)$ between the remote vehicles i and $i+1$ under their worst-case behaviors, $\delta(t)$ describes the time evolution of the largest possible rear gap $h_{0,i+1}$ such that the smallest necessary front gap s_{F} is secured for a lane change. Thus, from the definition (35), the set Γ_{env} collects the time t and rear gap values $h_{0,i+1}$ that satisfy the proposition $\tilde{M}_i$ under the worst *environmental* behaviors; see the orange shaded region in Fig. 5(b). The set Γ_{env} quantifies the lane change opportunity provided by the worst-case environment, regardless of whether the ego vehicle is able to seize it. The ego vehicle's motion capability is captured by the other set, Γ_{ego}, that will be explained further below. This way, we decoupled the environmental behaviors from the ego agent's dynamics, which reduces the dimension involved in the calculation. Moreover, the consideration of the remote vehicles' worst-case behaviors, justified by Lemma 1, filtered out unnecessary environmental uncertainties.

The set Γ_{ego} in (36) gives all rear gap values that the ego vehicle is able to reach along the time $t \geq t_k$; see the light purple shaded region in Fig. 5(b). This set is the projection of the reachable tube of system (1) from the 6D time-space domain $\mathbb{R} \times \tilde{\Omega}_i$ onto the 2D $(t, h_{0,i+1})$-plane. We emphasize that by projecting the reachable tube to a lower-dimensional space, we bypassed the dimensionality challenges associated with reachability analysis. Moreover, such a projected tube can be calculated straightforwardly using a lower bound $h_{0,i+1}^{\min}(t)$ and an upper bound $h_{0,i+1}^{\max}(t)$; see the blue and red curves in Fig. 5(b). We remark that the calculation of these bounds uses the ego vehicle's control input history $u_0(t)$ along $t \in [t_k - \sigma, t_k]$ due to the time delay σ in its dynamics. This input history is known at the time t_k. Following these, the intersection Γ in (34) gives all reachable rear gaps $h_{0,i+1}$ and the corresponding time t to satisfy the proposition $\tilde{M}_i$; see the striped region in Fig. 5(b). By Lemma 1, $\Gamma \neq \emptyset$ is equivalent to $\tilde{\mathbf{x}}_i(t_k) \in \tilde{\mathcal{M}}_{\mathrm{g}}^i$, and the ego vehicle shall confidently pursue a conflict-free lane change. We refer to Γ the lane change opportunity set. The conflict chart in Fig. 5(a) highlights two system states indicated by points A and B, whose opportunity sets Γ are constructed in Fig. 5(b) and (c) respectively. The state A has a non-empty set Γ and thus $\mathrm{A} \in \tilde{\mathcal{M}}_{\mathrm{g}}^i$, while the state B has an empty set Γ, leading to $\mathrm{B} \notin \tilde{\mathcal{M}}_{\mathrm{g}}^i$.

The emptiness of the set Γ is checked along $t \geq t_k$ at each integration time step as $\delta(t)$, $h_{0,i+1}^{\min}(t)$, and $h_{0,i+1}^{\max}(t)$ are calculated. The time complexity of checking the set Γ is thus linear in the number of integration time steps. Condition $t \geq t_k$ in (35) and (36) indicates that the sets Γ_{env} and Γ_{ego} may not be bounded in the time domain. Our previous work [34] shows that condition (33) results in a bounded time horizon, during which $[s_{\mathrm{R}}, \delta(t)]$ remains non-empty so the set Γ can be constructed. If condition (33) does not hold, one may impose a sufficiently large but finite end time for checking the set Γ, by which the ego vehicle intends to initiate a lane change.

Applying the same approach, the following Theorem provides a criterion to check $\tilde{\mathbf{x}}_i(t_k) \in \tilde{\mathcal{M}}_{\mathrm{r}}^i$.

Theorem 3: Given the dynamics (1)-(2) and the state $\tilde{\mathbf{x}}_i(t_k) \in \tilde{\Omega}_i$, $\tilde{\mathbf{x}}_i(t_k) \in \tilde{\mathcal{M}}_{\mathrm{r}}^i$ holds if and only if the condition

$$\hat{\Gamma} := \Gamma_{\mathrm{env}} \cap \Gamma_{\mathrm{ego}} = \emptyset, \tag{38}$$

is satisfied under $(u_i(t), u_{i+1}(t)) \equiv (\overline{u}_i(t), \underline{u}_{i+1}(t))$, for the Γ_{env} and Γ_{ego} defined in (35) and (36).

Proof: See Appendix E. □

One may notice from (38) that the set $\hat{\Gamma}$ shares the same definition as the set Γ in (34), but its calculation involves a different set of condition for the input pair $(u_i(t), u_{i+1}(t))$. The notation $\hat{\Gamma}$ is used to distinguish such a difference from Γ. Theorem 3 states that the lane change opportunity set $\hat{\Gamma}$ being empty under the remote vehicles' best-case behaviors is equivalent to $\tilde{\mathbf{x}}_i(t_k) \in \tilde{\mathcal{M}}_{\mathrm{r}}^i$, i.e., a conflict-free lane change between remote vehicles i and $i+1$ is not possible for the ego vehicle. The use of the remote vehicles' best-case behaviors is justified by Lemma 2. Fig. 5(d) constructs such a best-case set $\hat{\Gamma}$ for the system state B, where $\hat{\Gamma} \neq \emptyset$ yields $\mathrm{B} \notin \tilde{\mathcal{M}}_{\mathrm{r}}^i$. The fact that $\mathrm{B} \notin \tilde{\mathcal{M}}_{\mathrm{g}}^i \cup \tilde{\mathcal{M}}_{\mathrm{r}}^i$ indicates that $\mathrm{B} \in \tilde{\mathcal{M}}_{\mathrm{y}}^i$; see Fig. 5(a). That is, a conflict-free lane change is uncertain. Again, under the parameter condition (33), $\tilde{\mathcal{M}}_{\mathrm{r}}^i = \emptyset$ always holds in lane change scenarios [34].

In summary, Theorems 2 and 3 efficiently convert the examination of $\tilde{\mathbf{x}}_i(t_k) \in \tilde{\mathcal{M}}_{\mathrm{g}}^i$ and $\tilde{\mathbf{x}}_i(t_k) \in \tilde{\mathcal{M}}_{\mathrm{r}}^i$ to the emptiness check of the lane change opportunity sets Γ and $\hat{\Gamma}$, which are constructed by set intersections. The efficiency of this approach is achieved by decoupling the environmental behaviors from the ego vehicle's dynamics and by projecting the system's reachable tube onto a lower-dimensional domain.

B. Conflict Analysis With Finite Merge Zone

So far we investigated the conflict analysis in lane change scenarios. A lane change can be viewed as a special case of a merge where the merge zone is infinitely large. In this section, we add back the geometrical constraint on merge zone, i.e., assume that the conditions $\underline{s} \to -\infty$ and $\overline{s} \to \infty$ no longer holds. We emphasize that this merge problem is space- and time-critical as the ego vehicle must seize the opportunity while remaining inside a specific position range. Note that this also adds one dimension back to our analysis, because the absolute position r_0 of the ego vehicle becomes important. Recall that in this case, the system state $\mathbf{x}_i$ lives in the 6D state space Ω_i, cf. (15) and (16). We show that the approach developed so far can be extended to accommodate the additional constraint.

Before developing the theory, we showcase an example of the sets $\mathcal{M}_{\mathrm{g}}^i$, $\mathcal{M}_{\mathrm{y}}^i$, and $\mathcal{M}_{\mathrm{r}}^i$ corresponding to a merge scenario in the $(h_{i,0}, h_{0,i+1})$-plane in Fig. 5(e). This chart is still referred to as conflict chart. We emphasize that compared to the pure lane change case in Fig. 5(a), where the conflict set was empty, here the red region indeed shows up due to having stricter maneuver constraints, i.e., $\mathcal{M}_{\mathrm{r}}^i \neq \emptyset$. In this example, except for an additionally imposed finite merge zone, the vehicles' states remain the same as in the lane change scenario in Fig. 5(a).

To check whether the system state $\mathbf{x}_i(t_k) \in \mathcal{M}_{\mathrm{g}}^i$, $\mathcal{M}_{\mathrm{y}}^i$, or $\mathcal{M}_{\mathrm{r}}^i$, we reuse the lane change opportunity sets Γ and $\hat{\Gamma}$ developed in Theorems 2 and 3. Notice that the set Γ can be alternatively written in the following form.

$$\Gamma = \bigcup_{t \geq t_k} t \times [\underline{\Gamma}(t), \overline{\Gamma}(t)], \tag{39}$$

where $\underline{\Gamma}(t) = \max\{s_{\mathrm{R}}, h_{0,i+1}^{\min}(t)\}$ and $\overline{\Gamma}(t) = \min\{\delta(t), h_{0,i+1}^{\max}(t)\}$ describe the lower and upper bounds of the set Γ at time t. Note that the set Γ is defined only at the times t when $\underline{\Gamma}(t) \leq \overline{\Gamma}(t)$ holds. By transforming the set Γ from $(t, h_{0,i+1})$-domain to (t, r_0)-domain, a criterion to check $\mathbf{x}_i(t_k) \in \mathcal{M}_{\mathrm{g}}^i$ is provided by the following Theorem.

Theorem 4: Given the dynamics (1)-(2) and the state $\mathbf{x}_i(t_k) \in \Omega_i$, $\mathbf{x}_i(t_k) \in \mathcal{M}_{\mathrm{g}}^i$ holds if and only if the condition

$$\Theta := \Gamma^* \cap \bigcup_{t \in [t_k, t_{\max,0}]} t \times [\underline{s}, \overline{s}] \neq \emptyset, \tag{40}$$

is satisfied under $(u_i(t), u_{i+1}(t)) \equiv (\underline{u}_i(t), \overline{u}_{i+1}(t))$, where

$$\Gamma^* := \bigcup_{t \in [t_k, t_{\max,0}]} t \times [\underline{\Gamma}(t) + r_{i+1}(t) + l, \overline{\Gamma}(t) + r_{i+1}(t) + l]. \tag{41}$$

Proof: See Appendix F. □

To understand the physical meaning of the set Θ defined in (40), we first recall from the definition (8) of rear gap $h_{0,i+1}$ that $r_0 = h_{0,i+1} + r_{i+1} + l$. Noting that the set Γ is expressed in terms of $h_{0,i+1}$, one confirms from (39) and (41) that the set Γ^* is in fact the set Γ transformed from $(t, h_{0,i+1})$-plane to (t, r_0)-plane, on the time domain $t \in [t_k, t_{\max,0}]$; see the cyan shaded region in Fig. 5(f). The set Γ^* thus gives all feasible values of the position r_0 that the ego vehicle is able to reach, and the corresponding time $t \in [t_k, t_{\max,0}]$ such that $h_{i,0}(t) \geq s_{\mathrm{F}} \wedge h_{0,i+1}(t) \geq s_{\mathrm{R}}$ holds under the worst-case behaviors of remote vehicles. Thus, the intersection Θ of the sets Γ^* and $\bigcup_{t\in[t_k,t_{\max,0}]} t \times [\underline{s}, \overline{s}]$ gives all feasible r_0 values and the corresponding times such that $h_{i,0}(t) \geq s_{\mathrm{F}} \wedge h_{0,i+1}(t) \geq s_{\mathrm{R}} \wedge r_0(t) \in [\underline{s}, \overline{s}]$ holds. Therefore, based on Theorem 2, $\Theta \neq \emptyset$ is equivalent to the ego vehicle being able to secure the necessary front and rear gaps inside the merge zone independent of the remote vehicles' behaviors, that is, $\mathbf{x}_i(t_k) \in \mathcal{M}_{\mathrm{g}}^i$. One such example is given in Fig. 5(f) for the state point A in Fig. 5(e). In contrast, $\Gamma = \emptyset$ leads to $\Theta = \emptyset$ for the state point B; see Fig. 5(c) and (g). Thus, $\mathrm{B} \notin \mathcal{M}_{\mathrm{g}}^i$ as shown in Fig. 5(e). We refer to the set Θ as the merge opportunity set, as opposed to the lane change opportunity set Γ. We remark again that here, the time delay σ in the ego vehicle's dynamics is taken into account when the set Γ is constructed.

Similarly, the set $\hat{\Gamma}$ can also be written in the form of (39), with the same definitions for $\underline{\Gamma}(t)$ and $\overline{\Gamma}(t)$, but subject to the best-case input pair $(u_i(t), u_{i+1}(t))$ given in the Theorem 3. The set $\hat{\Gamma}^*$ is then given by (41) using such $\underline{\Gamma}(t)$ and $\overline{\Gamma}(t)$. By constructing the set $\hat{\Gamma}$ and accordingly, the set $\hat{\Gamma}^*$, one derives a similar criterion to check $\mathbf{x}_i(t_k) \in \mathcal{M}_{\mathrm{r}}^i$, given by the following Theorem.

Theorem 5: Given the dynamics (1)-(2) and the state $\mathbf{x}_i(t_k) \in \Omega$, $\mathbf{x}_i(t_k) \in \mathcal{M}_{\mathrm{r}}^i$ holds if and only if the condition

$$\hat{\Theta} := \hat{\Gamma}^* \cap \bigcup_{t\in[t_k,t_{\max,0}]} t \times [\underline{s}, \overline{s}] = \emptyset, \tag{42}$$

is satisfied under $(u_i(t), u_{i+1}(t)) \equiv (\overline{u}_i(t), \underline{u}_{i+1}(t))$.

Proof: See Appendix G. □

That is, the merge opportunity set $\hat{\Theta}$ being empty under the remote vehicles' best-case behaviors is equivalent to the ego vehicle being unable to secure the necessary front and rear gaps inside the merge zone, i.e., $\mathbf{x}_i(t_k) \in \mathcal{M}_{\mathrm{r}}^i$. Fig. 5(d) and (h) illustrate an example of the sets $\hat{\Gamma}$ and $\hat{\Gamma}^*$ under the indicated conditions such that $\hat{\Theta} = \emptyset$. This corresponds to the state point $\mathrm{B} \in \mathcal{M}_{\mathrm{r}}^i$ depicted in Fig. 5(e).

As exemplified by Fig. 5(d), the set $\hat{\Gamma}$ (and similarly, Γ) may be unbounded depending on the input limits of remote vehicles, but the consideration of a finite time window $[t_k, t_{\max,0}]$ ensures that the set $\hat{\Gamma}^*$ (and similarly, Γ^*) is always bounded; see Fig. 5(h), thereby avoiding infinite (and unnecessary) set calculation. We also emphasize that the construction of the sets Θ and $\hat{\Theta}$ is highly efficient as the sets Γ^* and $\hat{\Gamma}^*$ are transformed from Γ and $\hat{\Gamma}$ under a straightforward algebraic calculation, and checking their intersections with the set $\bigcup_{t\in[t_k,t_{\max,0}]} t \times [\underline{s}, \overline{s}]$ remains numerically fast.

Comparing the conflict charts in the $(h_{i,0}, h_{0,i+1})$-plane in Fig. 5(a) and (e), the green no-conflict region shrinks while the red conflict region expands (from empty) under the additional geometrical constraint associated with the merge zone. This can be formally expressed by the following Corollary.

Corollary 1: Given the dynamics (1)-(2). The following relationships hold between the no-conflict sets $\mathcal{M}_{\mathrm{g}}^i$ and $\tilde{\mathcal{M}}_{\mathrm{g}}^i$, and the conflict sets $\mathcal{M}_{\mathrm{r}}^i$ and $\tilde{\mathcal{M}}_{\mathrm{r}}^i$:

$$Proj_{\Omega_i \to \tilde{\Omega}_i}(\mathcal{M}_{\mathrm{g}}^i) \subseteq \tilde{\mathcal{M}}_{\mathrm{g}}^i, \tag{43}$$

$$Proj_{\Omega_i \to \tilde{\Omega}_i}(\mathcal{M}_{\mathrm{r}}^i) \supseteq \tilde{\mathcal{M}}_{\mathrm{r}}^i, \tag{44}$$

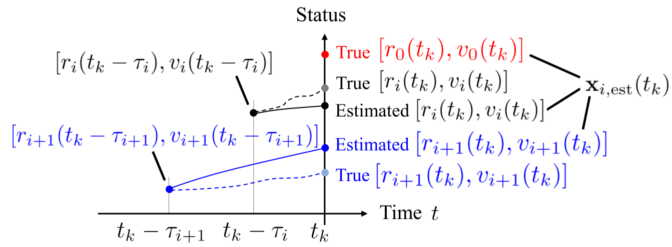

Fig. 6. A conceptual illustration of estimating current system state at time t_k to account for the communication delays τ_i and τ_{i+1} in conflict analysis. The dashed curves depict the remote vehicles' actual behaviors, whereas the solid curves represent the estimates derived from (46)-(47) or (50)-(51).

where $Proj_{\Omega_i \to \tilde{\Omega}_i}(\cdot)$ is a projection operator that projects a set from the 6D domain Ω_i to the 5D domain $\tilde{\Omega}_i$.

Noting that the only difference between the domains Ω_i and $\tilde{\Omega}_i$ is an extra dimension r_0, the projection simply removes the r_0 elements from the sets $\mathcal{M}_{\mathrm{g}}^i$ and $\mathcal{M}_{\mathrm{r}}^i$, making the comparison with the sets $\tilde{\mathcal{M}}_{\mathrm{g}}^i$ and $\tilde{\mathcal{M}}_{\mathrm{r}}^i$ feasible. The relationship (43) is derived from Theorems 2 and 4, while (44) is derived from Theorems 3 and 5.

To summarize, Theorems 4 and 5 reveal that a simple adaptation of the reachability-based approach developed in the previous subsection allows for efficient study of conflicts under stricter maneuver constraints. This demonstrates the scalability and efficient implementability of the conflict analysis framework. By applying these Theorems to check the states within the set Ω_i, one obtains the conflict chart; see Fig. 5(e).

In practice, however, the ego vehicle does not necessarily have to construct the whole conflict chart, but may simply check which subset the current system state is in. Based on this, the ego vehicle's maneuver decision can be made. If $\mathbf{x}_i(0) \in \mathcal{M}_{\mathrm{g}}^i$, then the ego vehicle shall pursue the opportunity to merge. If $\mathbf{x}_i(t_k) \in \mathcal{M}_{\mathrm{r}}^i$, then a conflict-free merge is not possible and the ego vehicle shall not merge between these two remote vehicles. If, however, $\mathbf{x}_i(t_k) \notin \mathcal{M}_{\mathrm{g}}^i \cup \mathcal{M}_{\mathrm{r}}^i$, then $\mathbf{x}_i(t_k) \in \mathcal{M}_{\mathrm{y}}^i$ holds. In this case, a conflict-free merge is not guaranteed. Thus, the ego vehicle shall still decide not to merge between the two remote vehicles.

C. Conflict Analysis Under Communication Delays

Our analysis so far ignored the time delays in communication. As shown in Fig. 6, when delays τ_i and τ_{i+1} exist in the V2X information from the remote vehicles i and $i+1$, the status information received by the ego vehicle at time t_k contains $[r_i(t_k-\tau_i), v_i(t_k-\tau_i), r_{i+1}(t_k-\tau_i), v_{i+1}(t_k-\tau_i)]$. The actual state $\mathbf{x}_i(t_k)$ thus becomes unavailable. Moreover, the intent information (5) is also delayed, covering a shifted time horizon given in (6).

However, the following relationship reveals that it is sufficient to use an appropriately estimated current state $\mathbf{x}_{i,\mathrm{est}}(t_k)$ to reason about if $\mathbf{x}_i(t_k) \in \mathcal{M}_{\mathrm{g}}^i$ holds.

$$\mathbf{x}_{i,\mathrm{est}}(t_k) \in \mathcal{M}_{\mathrm{g}}^i \implies \mathbf{x}_i(t_k) \in \mathcal{M}_{\mathrm{g}}^i, \tag{45}$$

where $\mathbf{x}_{i,\mathrm{est}}(t_k)$ is the estimated state calculated using

$$u_i(t) = \begin{cases} \underline{a}_i(t), & \text{if } t \in [t_k - \tau_i, \min\{t_k, t_k + T_i - \tau_i\}), \\ a_{\min,i}, & \text{if } t \in [\min\{t_k, t_k + T_i - \tau_i\}, t_k), \end{cases} \tag{46}$$

$$u_{i+1}(t) = \begin{cases} \overline{a}_{i+1}(t), & \text{if } t \in [t_k - \tau_{i+1}, \min\{t_k, t_k + T_{i+1} - \tau_{i+1}\}), \\ a_{\max,i+1}, & \text{if } t \in [\min\{t_k, t_k + T_{i+1} - \tau_{i+1}\}, t_k). \end{cases} \tag{47}$$

Here, (46)-(47) prescribe the remotes vehicles' worst-case behaviors over their communication delay intervals, which is necessary to accommodate the most adversarial situation; see Fig. 6 for a conceptual representation. This estimation leads to an estimated merge opportunity set Θ that is never larger than the actual one. The relationship (45) thus follows.

Note that Theorem 4 still holds when replacing $(u_i(t), u_{i+1}(t)) \equiv (\underline{u}_i(t), \overline{u}_{i+1}(t))$ with

$$u_i(t) = \begin{cases} \underline{a}_i(t), & \text{if } t \in [t_k, \max\{t_k, t_k + T_i - \tau_i\}), \\ a_{\min,i}, & \text{otherwise}, \end{cases} \tag{48}$$

$$u_{i+1}(t) = \begin{cases} \overline{a}_{i+1}(t), & \text{if } t \in [t_k, \max\{t_k, t_k + T_{i+1} - \tau_{i+1}\}), \\ a_{\max,i+1}, & \text{otherwise}, \end{cases} \tag{49}$$

which correspond to the worst-case future motion of remote vehicles based on their delayed intent. This way, although the actual state $\mathbf{x}_i(t_k)$ is unknown, $\mathbf{x}(t_k) \in \mathcal{M}_{\mathrm{g}}^i$ can be inferred by checking $\mathbf{x}_{i,\mathrm{est}}(t_k) \in \mathcal{M}_{\mathrm{g}}^i$.

Similarly, by constructing $\mathbf{x}_{i,\mathrm{est}}(t_k)$ using

$$u_i(t) = \begin{cases} \overline{a}_i(t), & \text{if } t \in [t_k - \tau_i, \min\{t_k, t_k + T_i - \tau_i\}), \\ a_{\max,i}, & \text{if } t \in [\min\{t_k, t_k + T_i - \tau_i\}, t_k), \end{cases} \tag{50}$$

$$u_{i+1}(t) = \begin{cases} \underline{a}_{i+1}(t), & \text{if } t \in [t_k - \tau_{i+1}, \min\{t_k, t_k + T_{i+1} - \tau_{i+1}\}), \\ a_{\min,i+1}, & \text{if } t \in [\min\{t_k, t_k + T_{i+1} - \tau_{i+1}\}, t_k), \end{cases} \tag{51}$$

one obtains

$$\mathbf{x}_{i,\mathrm{est}}(t_k) \in \mathcal{M}_{\mathrm{r}}^i \implies \mathbf{x}_i(t_k) \in \mathcal{M}_{\mathrm{r}}^i. \tag{52}$$

Here, (50)-(51) represent the remote vehicles' best-case behaviors on their communication delay intervals; see Fig. 6 for a conceptual illustration.

Note that Theorem 5 also holds when replacing $(u_i(t), u_{i+1}(t)) \equiv (\overline{u}_i(t), \underline{u}_{i+1}(t))$ with

$$u_i(t) = \begin{cases} \overline{a}_i(t), & \text{if } t \in [t_k, \max\{t_k, t_k + T_i - \tau_i\}), \\ a_{\max,i}, & \text{otherwise}, \end{cases} \tag{53}$$

$$u_{i+1}(t) = \begin{cases} \underline{a}_{i+1}(t), & \text{if } t \in [t_k, \max\{t_k, t_k + T_{i+1} - \tau_{i+1}\}), \\ a_{\min,i+1}, & \text{otherwise}, \end{cases} \tag{54}$$

which correspond to the best-case future motion of remote vehicles based on their delayed intent.

Thus, the efficiency of conflict analysis under stricter maneuver constraints is preserved when incorporating communication delays. Examples of dealing with communication delays will be given in the next section using real traffic data.

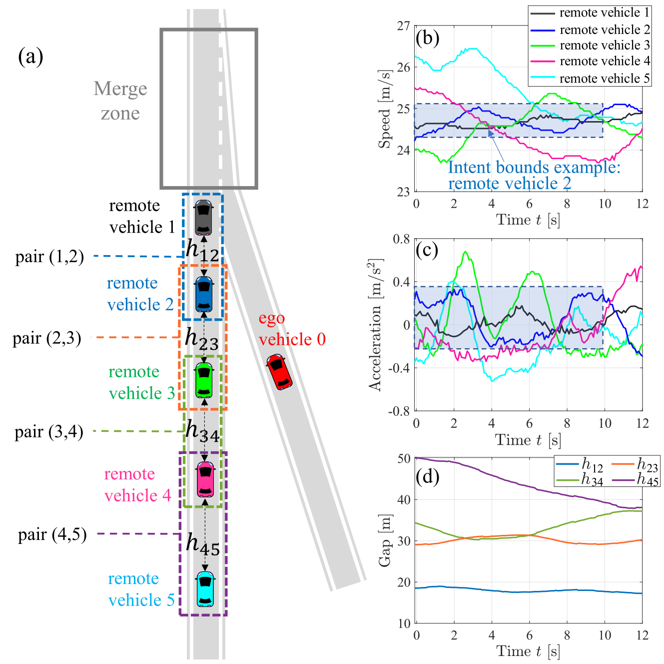

Fig. 7. Real highway data of a chain of remote vehicles driving towards a merge zone. (a) Conceptual illustration. (b)-(c) Remote vehicles' speed and acceleration profiles. (d) Inter-vehicle distances of each remote vehicle pair.

V. Controller Design and Simulation

In the previous sections, we developed scalable approaches that reduce a global conflict management problem to efficiently solvable pairwise local conflict analysis. This section starts with controller design. We then combine our earlier discussions to demonstrate the effectiveness of the whole framework via simulations driven by real highway data.

A. Goal-Oriented Control

For $\mathbf{x}_i(t_k) \in \mathcal{M}_{\mathrm{g}}^i$ (or $\mathbf{x}_{i,\mathrm{est}}(t_k) \in \mathcal{M}_{\mathrm{g}}^i$ under communication delays), we have a non-empty merge opportunity set Θ; see Theorem 4. Each point in this set, $(t, r_0) \in \Theta$, provides a feasible position and a corresponding time for the ego vehicle's conflict-free merge. Therefore, one can design the control input $u_0(t)$ by selecting an appropriate goal point $(t^{\mathrm{G}}, r_0^{\mathrm{G}}) \in \Theta$ for the ego vehicle to pursue. Note that the goal point can be updated at each time t_k when the latest V2X information from remote vehicles is received. Such a controller is referred to as goal-oriented controller. We remark that the idea of goal-oriented control design was originally proposed in our earlier work [43] for the pure lane change scenarios mentioned in the Section IV-A. In what follows, we extend the framework of goal-oriented controller to multi-vehicle merge scenarios. We then demonstrate its applicability in larger traffic scale in the next subsection.

A control designer may select different goal points in the set Θ to achieve various desired ego vehicle performances, e.g., to optimize time/energy efficiency and passenger comfort. Here, to achieve better robustness, we choose the goal point to be the "center" of the opportunity set, that is, we select t^{G} in the middle of the time span of the set Θ and r_0^{G} in

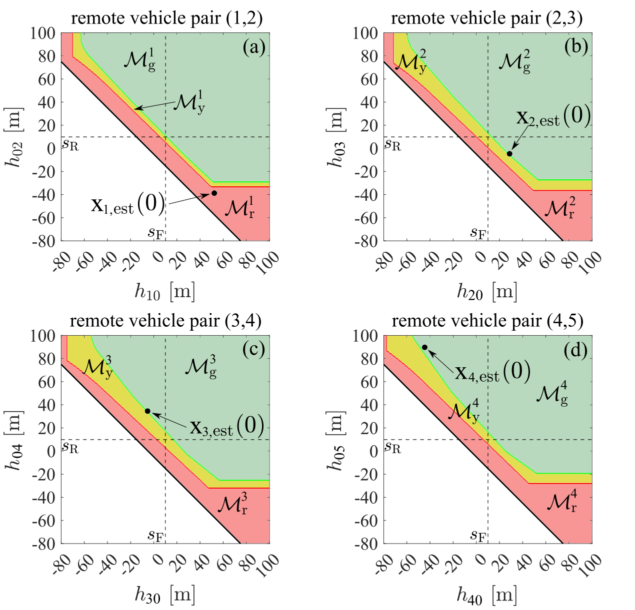

Fig. 8. Conflict charts in the plane of front and rear gaps. Each chart corresponds to a different remote vehicle pair in Fig. 7 at time $t_k = 0$, under the delay $\sigma = 0.5$ [s] in the ego vehicle's dynamics and delay $\tau = 0.1$ [s] in the remote vehicles' V2X information, for velocities (a) $v_0(0), v_1(-0.1), v_2(-0.1)$; (b) $v_0(0), v_2(-0.1), v_3(-0.1)$; (c)$v_0(0), v_3(-0.1), v_4(-0.1)$; and (d) $v_0(0), v_4(-0.1), v_5(-0.1)$; see the delayed velocity values in Table III. Here, the ego vehicle's initial position and velocity are given as $r_0(0) = 0$ [m] and $v_0(0) = 25$ [m/s], respectively, and the merge zone is located at $[100, 200]$ [m]. Table IV summarizes the estimated initial state encoded in $\mathbf{x}_{i,\mathrm{est}}(0)$ $(i = 1, \ldots, 4)$ for panels (a)-(d).

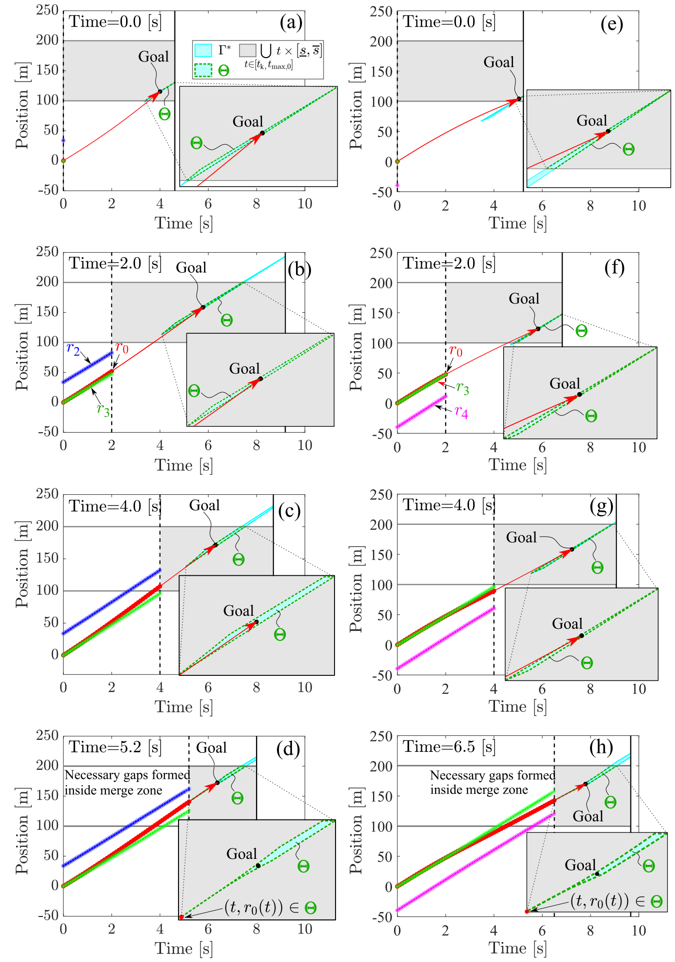

Fig. 9. (a)-(d) Evolution of merge opportunity set Θ, goal point $(t^{\mathrm{G}}, r_0^{\mathrm{G}}) \in \Theta$, and positions r_0, r_2, and r_3, corresponding to the merge scenario in Fig. 7. Here, the ego vehicle 0 pursues merge opportunity between remote vehicles 2 and 3 using goal-oriented controller $u_0(t) = u_0^{\mathrm{G}}$ with status and intent updates every 0.1[s]. (e)-(h) The corresponding evolution when the ego vehicle pursues an alternative merge opportunity between remote vehicles 3 and 4 using a goal oriented controller.

the middle of the slice $\Theta(t^{\mathrm{G}})$; see the black dot in Fig. 9(a) for an example of a goal point. Accommodating time delays in both vehicle dynamics and communication, we design a goal-oriented control input of constant value, i.e., $u_0(t) = u_0^{\mathrm{G}}$, with which the goal point $(t^{\mathrm{G}}, r_0^{\mathrm{G}}) \in \Theta$ can be pursued by the ego vehicle. The analytical expression of u_0^{G} is given in Appendix H. Under this constant-value input, the expected trajectory $r_0(t)$ is illustrated in Fig. 9(a) by the red arrow. Such controller provides guarantees on the control feasibility of forming necessary front and rear gaps inside the merge zone. That is, it renders the green no-conflict set $\mathcal{M}_{\mathrm{g}}^i$ control invariant. When updated status and intent information is received from the remote vehicles, the ego vehicle may recompute the opportunity set Θ, update the goal point $(t^{\mathrm{G}}, r_0^{\mathrm{G}}) \in \Theta$, and recalculate the corresponding goal-oriented control input u_0^{G}; see Fig. 9(b)–(d).

B. Data-Driven Multi-Vehicle Simulation

So far, we have developed all necessary tools to manage conflicts in multi-vehicle merge; see Fig. 1(a), which involves an ego vehicle and N remote vehicles. In this subsection, we demonstrate the framework using a real-data-driven simulation with $N = 5$.

As shown in Fig. 7(a), 4 pairs of remote vehicles exist. Following the idea of pairwise conflict analysis, the ego vehicle shall perform conflict analysis sequentially with each pair of remote vehicles from the pair $(1, 2)$ to the pair $(4, 5)$. The farthest pair ahead, $(i, i+1)$, whose status and intent yield $\mathbf{x}_i(t_k) \in \mathcal{M}_{\mathrm{g}}^i$ (or $\mathbf{x}_{i,\mathrm{est}}(t_k) \in \mathcal{M}_{\mathrm{g}}^i$ if communication delays exist), shall be selected as target vehicles to pursue a conflict-free merge. Again, such selection maximizes the ego vehicle's time efficiency since this guarantees a faster merging time.

To demonstrate pairwise conflict analysis, we represent the motion of the five remote vehicles using real data collected on the highway US-23 in south-east Michigan. Fig. 7(b)-(d) show the profiles of the remote vehicles' speeds, accelerations, and inter-vehicle distances h_{12}, h_{23}, h_{34}, and h_{45}. Note that the speeds and accelerations in Fig. 7(b,d) were obtained by smoothing the raw data with a 3rd order Savitsky-Golay filter. Without loss of generality, we assume that all remote vehicles share their status and intent information synchronously every 0.1 [s], and the simulation's initial time $t = 0$ corresponds to a time t_k when the remote vehicles' V2X information is delivered to the ego vehicle. We also assume the ego vehicle 0 to be a connected automated vehicle with initial position $r_0(0) = 0$ [m] and initial speed $v_0(0) = 25$ [m/s].

The ego vehicle attempts to select a pair of remote vehicles to merge between, within the merge zone located at

TABLE III

INITIAL AND DELAYED STATUS OF REMOTE VEHICLES 1-5 IN FIG. 7

Initial status			
$r_1(0)$	57.3 [m]	$v_1(0)$	24.5 [m/s]
$r_2(0)$	33.7 [m]	$v_2(0)$	24.3 [m/s]
$r_3(0)$	-0.3 [m]	$v_3(0)$	24.0 [m/s]
$r_4(0)$	-39.6 [m]	$v_4(0)$	25.5 [m/s]
$r_5(0)$	-94.7 [m]	$v_5(0)$	26.2 [m/s]
Delayed status			
$r_1(-0.1)$	54.9 [m]	$v_1(-0.1)$	24.6 [m/s]
$r_2(-0.1)$	31.3 [m]	$v_2(-0.1)$	24.2 [m/s]
$r_3(-0.1)$	-2.7 [m]	$v_3(-0.1)$	24.0 [m/s]
$r_4(-0.1)$	-42.1 [m]	$v_4(-0.1)$	25.5 [m/s]
$r_5(-0.1)$	-97.3 [m]	$v_5(-0.1)$	26.3 [m/s]

TABLE IV

ESTIMATED STATE ENCODED IN $\mathbf{x}_{i,\mathrm{est}}(0)$ FOR EACH PANEL OF FIG. 8(A)

(a)	$(h^{\mathrm{est}}_{10}(0), h^{\mathrm{est}}_{02}(0)) = (52.3, -38.8)$ [m], $(v^{\mathrm{est}}_{1}(0), v^{\mathrm{est}}_{2}(0)) = (24.60, 24.22)$ [m/s].
(b)	$(h^{\mathrm{est}}_{20}(0), h^{\mathrm{est}}_{03}(0)) = (28.8, -4.7)$ [m], $(v^{\mathrm{est}}_{2}(0), v^{\mathrm{est}}_{3}(0)) = (24.22, 24.09)$ [m/s].
(c)	$(h^{\mathrm{est}}_{30}(0), h^{\mathrm{est}}_{04}(0)) = (-5.3, 34.6)$ [m], $(v^{\mathrm{est}}_{3}(0), v^{\mathrm{est}}_{4}(0)) = (23.99, 25.50)$ [m/s].
(d)	$(h^{\mathrm{est}}_{40}(0), h^{\mathrm{est}}_{05}(0)) = (-44.6, 89.7)$ [m], $(v^{\mathrm{est}}_{4}(0), v^{\mathrm{est}}_{5}(0)) = (25.47, 26.32)$ [m/s].

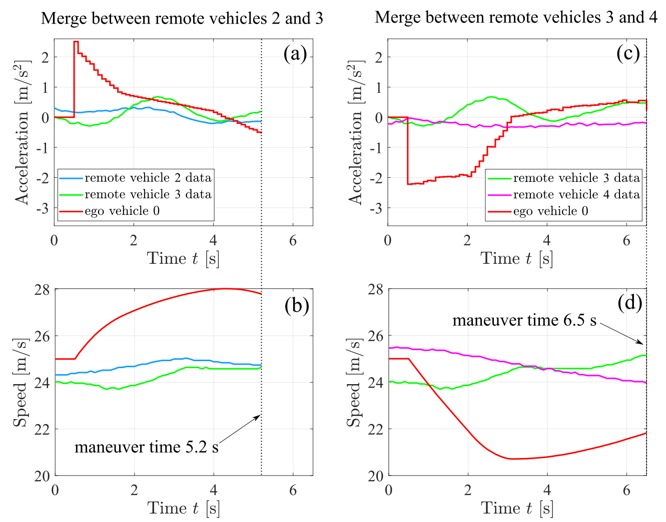

Fig. 10. (a)-(b) Simulation results of the ego vehicle 0 pursuing merge opportunity between remote vehicles 2 and 3, corresponding to Fig. 9(a)-(d). (c)-(d) Simulation results of the ego vehicle 0 pursuing an alternative (but less efficient) merge opportunity between remote vehicles 3 and 4, corresponding to Fig. 9(e)-(h).

[100, 200] [m]. Based on data, the remote vehicles' initial positions and speeds are given in Table III. That is, the ego vehicle initially travels near the remote vehicle 3 (in terms of longitudinal position); see Fig. 7(a) for a conceptual illustration. We consider the delay $\sigma = 0.5$ [s] in the ego vehicle's dynamics and the communication delay $\tau = 0.1$ [s] associated with all remote vehicles. At the initial time $t = 0$, the ego vehicle is aware of the remote vehicles' delayed status shown in Table III, as well as the remote vehicles' delayed intent shared at time $t = -0.1$ [s]. The remote vehicles' intent can be extracted from the data. An example of the remote vehicle 2's intent at $t = -0.1$ [s] with a 10 [s] horizon is visualized by the blue shadings in Fig. 7(b)-(c) over the time span of $[-0.1, 9.9]$ [s]. In addition, all remote vehicles' behavior limits follow the values in Table I.

At the initial time, the ego vehicle first estimates the remote vehicles' current status based on the discussion in Section IV-C. Then it performs pairwise conflict analysis according to Theorems 4 and 5 with each pair of remote vehicles sequentially. The conflict charts associated with the four possible pairs of remote vehicles are shown in Fig. 8(a)-(d) in the plane of front and rear gaps. In the conflict chart in Fig. 8(a), the estimated initial state $\mathbf{x}_{1,\mathrm{est}}(0)$ is in the conflict set $\mathcal{M}^1_{\mathrm{r}}$, if the remote vehicles 1 and 2 are considered. Therefore, the ego vehicle shall not decide to merge between remote vehicles 1 and 2. On the other hand, for remote vehicle pairs $(2, 3)$, $(3, 4)$, and $(4, 5)$, Fig. 8(c)-(d) reveal that we have $\mathbf{x}_{2,\mathrm{est}}(0) \in \mathcal{M}^2_{\mathrm{g}}$, $\mathbf{x}_{3,\mathrm{est}}(0) \in \mathcal{M}^3_{\mathrm{g}}$, and $\mathbf{x}_{4,\mathrm{est}}(0) \in \mathcal{M}^4_{\mathrm{g}}$. That is, conflict-free merge opportunities exist in all these remote vehicle pairs. For the best time efficiency, the ego vehicle shall select the pair $(2, 3)$ to pursue a conflict-free merge.

This decision is executed by the goal-oriented controller $u_0(t) = u^{\mathrm{G}}_0$. Under every 0.1 [s] update rate of V2X information, Fig. 9(a)-(d) show the evolution of the merge opportunity set Θ, goal point $(t^{\mathrm{G}}, r^{\mathrm{G}}_0) \in \Theta$, and the positions r_0, r_2, and r_3, as the ego vehicle 0 pursues its merge opportunity between the remote vehicles 2 and 3. Under the designed goal-oriented controller, at time $t = 5.2$ [s], the ego vehicle forms the necessary front and rear gaps while remaining inside the merge zone; see Fig. 9(d). This can be confirmed by noticing that $(t, r_0(t))) \in \Theta$ holds, and thus, $\mathbf{x}_2(t) \in \mathcal{M}^2_{\mathrm{g}}$ holds according to Theorems 4 and (45). The ego vehicle may then start its lateral motion to complete the merge maneuver. Notice that the goal point is functioning as a guidance for the ego vehicle's conflict-free and feasible maneuver, while it is not necessary to actually reach it. The ego vehicle's speed and acceleration profiles when merging between remote vehicles 2 and 3 are shown in Fig. 10(a)-(b).

We remark that the goal-oriented controller may also be applied for the ego vehicle to merge between the remote vehicle pairs $(3, 4)$ and $(4, 5)$ without a conflict, but choosing one of these pairs lead to worse time efficiency. For example, Fig. 9(e)-(h) depict the evolution of the merge opportunity set Θ, goal point $(t^{\mathrm{G}}, r^{\mathrm{G}}_0) \in \Theta$, and the positions r_0, r_3, and r_4 when the ego vehicle pursues a merge between remote vehicles 3 and 4 with a goal-oriented controller. In this case, $(t, r_0(t)) \in \Theta$ holds at the time $t = 6.5$ [s]. That is, the conflict-free merge condition is satisfied 1.3 [s] later than merging between remote vehicles 2 and 3. The corresponding acceleration and speed profiles during such a maneuver are shown in Fig. 10(c)-(d). Notice that merging between remote vehicles 3 and 4 requires the ego vehicle to reduce its speed. Thus, in addition to a longer maneuver time and a further behind merge position, the ego vehicle also ends up with a slower longitudinal speed when the necessary safety gaps are formed.

These results validate the benefits of merging between the farthest remote vehicle pair ahead that provides non-empty merge opportunity set. The effectiveness of goal-oriented control under the scalable conflict analysis framework is thus demonstrated.

VI. Conclusion

In this paper, we investigated the scalability of cooperative maneuvering through the lens of the conflict analysis framework. Methodological scalability was examined in a mixed-traffic environment with vehicles of different autonomy levels and cooperation capabilities. Time delays in vehicle dynamics and communication were also considered. We proposed pairwise conflict analysis, which decomposes a large-scale global conflict into smaller-scale local conflicts that can be solved sequentially in lower-dimensional problems with efficient numerical methods. Such efficiency was achieved through a well-designed reachability-based approach, which (i) decoupled the environmental uncertainties from the ego vehicle's behaviors and (ii) projected the system's reachable tube to lower-dimensional subspaces.

Conflict analysis on a complicated merge scenario was derived after an adaptation of the methodology built for a simpler lane change scenario. Real-time implementability was maintained during the extension. Across different scenarios and scales, conflict analysis preserves advantages such as simplicity in accommodating delay effects, capability of dealing with different V2X information, and flexibility in control design. These results were validated using simulations based on real traffic data in a multi-vehicle merge scenario.

Future research will explore a general solution for scenario-agnostic implementations of pairwise conflict analysis. The scalability of conflict analysis and goal-oriented control shall also be studied with other cooperation categories, such as negotiation, where vehicles actively seek maneuver agreements.

Appendix A
Proof of Theorem 1

We first prove (21).

($\Rightarrow$) The left hand side indicates that $\forall u_1(t),\dots,u_N(t)$, $\exists u_0, \exists t \geq 0, \exists i \in \{1,\dots,N-1\}$, $h_{i,0}(t) \geq s_{\rm F} \wedge h_{0,i+1}(t) \geq s_{\rm R} \wedge r_0(t) \in [\underline{s},\overline{s}]$. This immediately yields the right hand side.

($\Leftarrow$) Given the right hand side, let i^* denote such an $i \in \{1,\dots,N-1\}$ that $\forall u_{i^*}(t)$, $u_{i^*+1}(t)$, $\exists u_0(t)$, $\exists t \geq 0$, $h_{i^*,0}(t) \geq s_{\rm F} \wedge h_{0,i^*+1}(t) \geq s_{\rm R} \wedge r_0(t) \in [\underline{s},\overline{s}]$. The above condition that involves $h_{i^*,0}$ and h_{0,i^*+1} while considering all possible u_{i^*} and u_{i^*+1} shall hold independently of other remote vehicles' control inputs, i.e., $\forall u_i(t), i \notin \{i^*, i^*+1\}$. Therefore, the left hand side holds.

Now we prove (22).

($\Rightarrow$) Noting that the order of universal quantifiers ($\forall$) is exchangeable, the left hand side implies that $\forall i \in \{1,\dots,N-1\}$, $\forall u_1(t),\dots,u_N(t)$, $\forall u_0(t)$, $\forall t \geq 0$, we have $\neg(h_{i,0}(t) \geq s_{\rm F} \wedge h_{0,i+1}(t) \geq s_{\rm R} \wedge r_0(t) \in [\underline{s},\overline{s}])$. This immediately leads to the right hand side.

($\Leftarrow$) The right hand side indicates that $\forall i \in \{1,\dots,N-1\}$, $\forall u_i(t)$, $u_{i+1}(t)$, $\forall u_0(t)$, $\forall t \geq 0$, $\neg(h_{i,0}(t) \geq s_{\rm F} \wedge h_{0,i+1}(t) \geq s_{\rm R} \wedge r_0(t) \in [\underline{s},\overline{s}])$. This is equivalent to the left hand side based on the above proof of ($\Rightarrow$).

Appendix B
Proof of Lemma 1

Here we prove (23).

($\Rightarrow$) From the left hand side, we know that for $(u_i(t),u_{i+1}(t)) \equiv (\underline{u}_i(t),\overline{u}_{i+1}(t))$, $\exists u_0(t)$, $\exists t \geq t_k$, such that $h_{i,0}(t) \geq s_{\rm F} \wedge h_{0,i+1}(t) \geq s_{\rm R} \wedge r_0(t) \in [\underline{s},\overline{s}]$ holds. Such t must satisfy $t \in [t_k, t_{\max,0}]$, since $r_0(t) \in [\underline{s},\overline{s}]$ implies $t \in [t_k, t_{\max,0}]$. Thus, the right hand side holds.

($\Leftarrow$) The right hand side implies that for $(u_i(t),u_{i+1}(t)) \equiv (\underline{u}_i(t),\overline{u}_{i+1}(t))$, $\exists u_0(t)$, M_i. Let u_0^* and t^* denote an input u_0 and a time t such that $h_{i,0}(t^*) \geq s_{\rm F} \wedge h_{0,i+1}(t^*) \geq s_{\rm R} \wedge r_0(t^*) \in [\underline{s},\overline{s}]$ holds under $(u_i(t),u_{i+1}(t)) \equiv (\underline{u}_i(t),\overline{u}_{i+1}(t))$. Now consider any $(u_i(t),u_{i+1}(t)) \not\equiv (\underline{u}_i(t),\overline{u}_{i+1}(t))$ and the same u_0^*. $r_0(t^*)$ remains unchanged, while both $h_{i,0}(t^*) = r_i(t^*) - r_0(t^*)$ and $h_{0,i+1}(t^*) = r_0(t^*) - r_{i+1}(t^*)$ become larger. Thus, $h_{i,0}(t^*) \geq s_{\rm F} \wedge h_{0,i+1}(t^*) \geq s_{\rm R} \wedge r_0(t^*) \in [\underline{s},\overline{s}]$ still holds, i.e., the left hand side.

Appendix C
Proof of Lemma 2

Below we prove (27).

($\Rightarrow$) The left hand side implies that for $(u_i(t),u_{i+1}(t)) \equiv (\overline{u}_i(t),\underline{u}_{i+1}(t))$, we have $\forall u_0(t), \forall t \geq t_k$, $\neg(h_{i,0}(t) \geq s_{\rm F} \wedge h_{0,i+1}(t) \geq s_{\rm R} \wedge r_0(t) \in [\underline{s},\overline{s}])$. Hence, the right hand side holds for $t \in [t_k, t_{\max,0}]$.

($\Leftarrow$) We first note that $t \geq t_{\max,0}$ implies $r_0(t) \notin [\underline{s},\overline{s}]$. Thus, given the right hand side, we have $\forall u_0(t)$, $\forall t \geq t_k$, $\neg(h_{i,0}(t) \geq s_{\rm F} \wedge h_{0,i+1}(t) \geq s_{\rm R} \wedge r_0(t) \in [\underline{s},\overline{s}])$ under $(u_i(t),u_{i+1}(t)) \equiv (\overline{u}_i(t),\underline{u}_{i+1}(t))$. Moreover, for any $(u_1(t),u_2(t)) \not\equiv (\overline{u}_i(t),\underline{u}_{i+1}(t))$, both $h_{i,0}(t)$ and $h_{0,i+1}(t)$ become smaller under any given $u_0(t)$. Thus, $\neg(h_{i,0}(t) \geq s_{\rm F} \wedge h_{0,i+1}(t) \geq s_{\rm R} \wedge r_0(t) \in [\underline{s},\overline{s}])$ still holds. This proves the left hand side.

Appendix D
Proof of Theorem 2

If $\Gamma \neq \emptyset$, then according to the definition of Γ in (34), under $(u_i(t),u_{i+1}(t)) \equiv (\underline{u}_i(t),\overline{u}_{i+1}(t))$, one has $\exists u_0(t), \exists t \geq t_k, s_{\rm R} \leq h_{0,i+1}(t) \leq \delta(t)$. Substituting $\delta(t) = h_{i,i+1}(t) - s_{\rm F} - l$ gives $h_{0,i+1}(t) \leq h_{i,i+1}(t) - s_{\rm F} - l$, i.e., $s_{\rm F} \leq h_{i,0}(t)$. These and Lemma 1 yield $\tilde{\mathbf{x}}_i(0) \in \tilde{\mathcal{M}}_{\rm g}^i$.

If $\Gamma = \emptyset$, then under $(u_i(t),u_{i+1}(t)) \equiv (\underline{u}_i(t),\overline{u}_{i+1}(t))$, one has $\forall u_0(t), \forall t \geq t_k, \neg\{s_{\rm R} \leq h_{0,i+1}(t) \leq \delta(t)\}$, i.e., $\neg\{h_{i,0}(t) \geq s_{\rm F} \wedge h_{0,i+1}(t) \geq s_{\rm R}\}$. That is, $\forall u_0(t), \neg\tilde{M}_i$. This yields $\tilde{\mathbf{x}}_i(0) \notin \tilde{\mathcal{M}}_{\rm g}^i$.

Appendix E
Proof of Theorem 3

If $\hat{\Gamma} = \emptyset$ under $(u_i(t),u_{i+1}(t)) \equiv (\overline{u}_i(t),\underline{u}_{i+1}(t))$, then according to the definition of $\hat{\Gamma}$ in (38), we have $\forall u_0(t), \forall t \geq t_k, \neg\{s_{\rm R} \leq h_{0,i+1}(t) \leq \delta(t)\}$. That is, $\neg\{h_{i,0}(t) \geq s_{\rm F} \wedge h_{0,i+1}(t) \geq s_{\rm R}\}$ holds. Hence $\tilde{\mathbf{x}}_i(0) \in \tilde{\mathcal{M}}_{\rm r}^i$ from Lemma 2.

If $\hat{\Gamma} \neq \emptyset$ under $(u_i(t),u_{i+1}(t)) \equiv (\underline{u}_i(t),\overline{u}_{i+1}(t))$, then from its definition we have $\exists u_0(t)$, $\exists t \geq t_k$, $s_{\rm R} \leq h_{0,i+1}(t) \leq \delta(t)$, i.e., $h_{i,0}(t) \geq s_{\rm F} \wedge h_{0,i+1}(t) \geq s_{\rm R}$. Thus, the proposition $\tilde{M}_i$ holds. These yield $\tilde{\mathbf{x}}_i(0) \notin \tilde{\mathcal{M}}_{\rm r}^i$.

APPENDIX F
PROOF OF THEOREM 4

Here we prove (40).

($\Rightarrow$) $\Theta \neq \emptyset$ implies that for $(u_i(t), u_{i+1}(t)) \equiv (\underline{u}_i(t), \overline{u}_{i+1}(t))$, we have $\exists u_0(t)$, $\exists t \in [t_k, t_{\max,0}]$, $r_0(t) \in [\underline{s}, \overline{s}] \wedge r_0(t) \in \Gamma^*(t)$, where $\Gamma^*(t)$ denotes the slice of the set Γ^* at time t. From the definition of Γ^*, $r_0(t) \in \Gamma^*(t) \iff \Gamma(t) \neq \emptyset$, where $\Gamma(t)$ is the slice of the set Γ at a given time t. From this, one derives that $h_{i,0}(t) \geq s_{\mathrm{F}} \wedge h_{0,i+1}(t) \geq s_{\mathrm{R}}$ holds. These and Lemma 1 imply that $\mathbf{x}_i(0) \in \mathcal{M}_{\mathrm{g}}^i$.

($\Leftarrow$) We prove this by contrapositive. If $\Theta = \emptyset$, then under $(u_i(t), u_{i+1}(t)) \equiv (\underline{u}_i(t), \overline{u}_{i+1}(t))$, $\forall u_0(t)$, $\forall t \in [t_k, t_{\max,0}]$, $\neg(r_0(t) \in [\underline{s}, \overline{s}] \wedge r_0(t) \in \Gamma^*)$. That is, similar to the argument above, $\neg(r_0(t) \in [\underline{s}, \overline{s}] \wedge h_{i,0}(t) \geq s_{\mathrm{F}} \wedge h_{0,i+1}(t) \geq s_{\mathrm{R}})$ holds. Also, $\forall t \geq t_{\max,0}$, we always have $r_0(t) \notin [\underline{s}, \overline{s}]$. Therefore, for $(u_i(t), u_{i+1}(t)) \equiv (\underline{u}_i(t), \overline{u}_{i+1}(t))$, $\forall u_0(t)$, $\neg M_i$. This implies $\mathbf{x}_i(0) \notin \mathcal{M}_{\mathrm{g}}^i$.

APPENDIX G
PROOF OF THEOREM 5

Below we prove (42).

($\Rightarrow$) If $\hat{\Theta} = \emptyset$ under $(u_i(t), u_{i+1}(t)) \equiv (\overline{u}_i(t), \underline{u}_{i+1}(t))$, then $\forall u_0(t)$, $\forall t \in [t_k, t_{\max,0}]$, one obtains $\neg(r_0(t) \in [\underline{s}, \overline{s}] \wedge r_0(t) \in \hat{\Gamma}^*(t))$. Since $r_0(t) \in \hat{\Gamma}^*(t) \iff h_{i,0}(t) \geq s_{\mathrm{F}} \wedge h_{0,i+1}(t) \geq s_{\mathrm{R}}$, we have $\neg(r_0(t) \in [\underline{s}, \overline{s}] \wedge h_{i,0}(t) \geq s_{\mathrm{F}} \wedge h_{0,i+1}(t) \geq s_{\mathrm{R}})$. These and Lemma 2 imply that $\mathbf{x}_i(0) \in \mathcal{M}_{\mathrm{r}}^i$.

($\Leftarrow$) We prove this by contrapositive. If $\hat{\Theta} \neq \emptyset$ under $(u_i(t), u_{i+1}(t)) \equiv (\overline{u}_i(t), \underline{u}_{i+1}(t))$, then we have $\exists u_0(t)$, $\exists t \in [t_k, t_{\max,0}]$, $r_0(t) \in [\underline{s}, \overline{s}] \wedge r_0(t) \in \hat{\Gamma}^*(t)$. That is, $r_0(t) \in [\underline{s}, \overline{s}] \wedge h_{i,0}(t) \geq s_{\mathrm{F}} \wedge h_{0,i+1}(t) \geq s_{\mathrm{R}}$. Thus, for $(u_i(t), u_{i+1}(t)) \equiv (\overline{u}_i(t), \underline{u}_{i+1}(t))$, $\exists u_0(t), M_i$. This implies $\mathbf{x}_i(0) \notin \mathcal{M}_{\mathrm{r}}^i$.

APPENDIX H
GOAL -ORIENTED CONTROLLER u_0^{G}

Given a goal point $(t^{\mathrm{G}}, r_0^{\mathrm{G}}) \in \Theta$, we have

$$u_0^G = \begin{cases} \frac{2\left(s^G - (t^G - t_k - \alpha)v_0\right)}{\left(t^G - t_k - \alpha\right)^2}, & \text{if } s^G \in \left[\frac{(t^G - t_k - \alpha)(v_0 + v_{\min,0})}{2}, \frac{(t^G - t_k - \alpha)(v_0 + v_{\max,0})}{2}\right], \\ f_1\left(v_0, I^G, s^G\right), & \text{if } s^G \in \left[0, \frac{(t^G - t_k - \alpha)(v_0 + v_{\min,0})}{2}\right], \\ f_2\left(v_0, t^G, s^G\right), & \text{otherwise.} \end{cases} \tag{55}$$

Here, v_0 represents $v_0(t_k + \sigma)$, computed using the dynamics (1) and the ego vehicle's known control input history over $t \in [t_k - \sigma, t_k]$. Accordingly, $s^{\mathrm{G}} = r_0^{\mathrm{G}} - r_0(t_k + \sigma)$ denotes the distance that the ego vehicle shall travel for $t > t_k + \sigma$ to reach r_0^{G} at time t^{G}.

$$f_1(v_0, t^{\mathrm{G}}, s^{\mathrm{G}}) = \begin{cases} \dfrac{2(s^{\mathrm{G}} - (t^{\mathrm{G}} - t_k - \sigma)v_0)}{(t^{\mathrm{G}} - t_k - \sigma)^2}, & \text{if } a_{\min,0} \geq \frac{v_{\min,0} - v_0}{t^{\mathrm{G}} - t_k - \sigma}, \\ \dfrac{(v_0 - v_{\min,0})^2}{2((t^{\mathrm{G}} - t_k - \sigma)v_{\min,0} - s^{\mathrm{G}})}, & \text{otherwise,} \end{cases} \tag{56}$$

$$f_2(v_0, t^{\mathrm{G}}, s^{\mathrm{G}}) = \begin{cases} \dfrac{2(s^{\mathrm{G}} - (t^{\mathrm{G}} - t_k - \sigma)v_0)}{(t^{\mathrm{G}} - t_k - \sigma)^2}, & \text{if } a_{\max,0} \leq \frac{v_{\max,0} - v_0}{t^{\mathrm{G}} - t_k - \sigma}, \\ \dfrac{(v_0 - v_{\max,0})^2}{2((t^{\mathrm{G}} - t_k - \sigma)v_{\max,0} - s^{\mathrm{G}})}, & \text{otherwise.} \end{cases} \tag{57}$$

Notice that u_0^{G} in (55) is derived such that the ego vehicle travels the distance s^{G} over the time interval $(t_k + \sigma, t^{\mathrm{G}}]$, with speed saturations considered. If a goal point is selected such that $s^{\mathrm{G}} < 0$, then it can be reached before $t_k + \sigma$ under the delayed control input history, and thus u_0^{G} is not applied.

REFERENCES

[1] J. Wen, N. Lyu, Y. Guo, and J. Jinsihan, "Analysis of conflict risk causes in urban expressway diverging areas: Considering unobserved heterogeneity and their interactions," *Transp. Lett.*, vol. 18, no. 1, pp. 161–178, Jan. 2026.

[2] N. Lyu, S. Feng, and H. Wan, "A perspective from competitive-cooperative driving modes: Identification of vehicle merging behavior models and crash risk factors in merge zone," *Accident Anal. Prevention*, vol. 220, Sep. 2025, Art. no. 108153.

[3] W. Chu, K. Yang, S. Li, and X. Tang, "Motion planning for autonomous driving with real traffic data validation," *Chin. J. Mech. Eng.*, vol. 37, no. 1, pp. 1–13, Jan. 2024.

[4] H. Chi, P. Cai, D. Fu, J. Zhai, Y. Zeng, and B. Shi, "Spatiotemporal-restricted A algorithm as a support for lane-free traffic at intersections with mixed flows," *Green Energy Intell. Transp.*, vol. 3, no. 2, Apr. 2024, Art. no. 100159.

[5] A. Irshayyid, J. Chen, and G. Xiong, "A review on reinforcement learning-based highway autonomous vehicle control," *Green Energy Intell. Transp.*, vol. 3, no. 4, Aug. 2024, Art. no. 100156.

[6] Z. Wang, Z. Zhao, X. Xing, D. Xu, X. Kong, and L. Zhou, "Conflict-based cross-view consistency for semi-supervised semantic segmentation," in *Proc. IEEE/CVF Conf. Comput. Vis. Pattern Recognit. (CVPR)*, Jun. 2023, pp. 19585–19595.

[7] H. Ding, J. Gao, Y. Yuan, and Q. Wang, "FF-LPD: A real-time frame-by-frame license plate detector with knowledge distillation and feature propagation," *IEEE Trans. Image Process.*, vol. 33, pp. 3893–3906, 2024.

[8] X. Chen, F. Ma, Y. Wu, B. Han, L. Luo, and S. A. Biancardo, "MFMDepth: MetaFormer-based monocular metric depth estimation for distance measurement in ports," *Comput. Ind. Eng.*, vol. 207, Sep. 2025, Art. no. 111325.

[9] S. Zeadally, M. A. Javed, and E. B. Hamida, "Vehicular communications for ITS: Standardization and challenges," *IEEE Commun. Standards Mag.*, vol. 4, no. 1, pp. 11–17, Mar. 2020.

[10] J. Zhang, R. Zhan, Y. Wang, and X. Qu, "Optical communication based V2V for vehicle platooning," *Green Energy Intell. Transp.*, vol. 4, no. 4, Aug. 2025, Art. no. 100278.

[11] Y. Wang, Z. Hu, S. Lou, and C. Lv, "Interacting multiple model-based ETUKF for efficient state estimation of connected vehicles with V2V communication," *Green Energy Intell. Transp.*, vol. 2, no. 1, Feb. 2023, Art. no. 100044.

[12] J. Liu, D. Chen, and Q. Chen, "Changeable shared bus lane scheme for intersections based on lane signals," *Transp. Saf. Environ.*, vol. 4, no. 4, p. 024, Oct. 2022.

[13] Taxonomy and Definitions for Terms Related To Cooperative Driving Automation for On-Road Motor Vehicles, Standard J3216, 2021.

[14] K. X. Cai, T. Phan-Minh, S.-J. Chung, and R. M. Murray, "Rules of the road: Formal guarantees for autonomous vehicles with behavioral contract design," *IEEE Trans. Robot.*, vol. 39, no. 3, pp. 1853–1872, Jun. 2023.

[15] Y.-T. Lin, H. Hsu, S.-C. Lin, C.-W. Lin, I. H.-R. Jiang, and C. Liu, "Graph-based modeling, scheduling, and verification for intersection management of intelligent vehicles," *ACM Trans. Embedded Comput. Syst.*, vol. 18, no. 5s, pp. 1–21, Oct. 2019.

[16] C. Liu, C.-W. Lin, S. Shiraishi, and M. Tomizuka, "Distributed conflict resolution for connected autonomous vehicles," *IEEE Trans. Intell. Vehicles*, vol. 3, no. 1, pp. 18–29, Mar. 2018.

[17] X. Chen et al., "Sensing data supported traffic flow prediction via denoising schemes and ANN: A comparison," *IEEE Sensors J.*, vol. 20, no. 23, pp. 14317–14328, Dec. 2020.

[18] Taxonomy and Definitions for Terms Related to Driving Automation Systems for On-Road Motor Vehicles, Standard J3016, 2021.

[19] S. L. Herbert, S. Bansal, S. Ghosh, and C. J. Tomlin, "Reachability-based safety guarantees using efficient initializations," in *Proc. IEEE 58th Conf. Decis. Control (CDC)*, Dec. 2019, pp. 4810–4816.

[20] N. Mehdipour, M. Althoff, R. D. Tebbens, and C. Belta, "Formal methods to comply with rules of the road in autonomous driving: State of the art and grand challenges," *Automatica*, vol. 152, Jun. 2023, Art. no. 110692.

[21] V.-A. Le, H. M. Wang, G. Orosz, and A. A. Malikopoulos, "Coordination for connected automated vehicles at merging roadways in mixed traffic environment," in *Proc. 62nd IEEE Conf. Decis. Control (CDC)*, Dec. 2023, pp. 4150–4155.

[22] F. Yao, C. Sun, B. Lu, B. Wang, and H. Yu, "Mixture of experts framework based on soft actor-critic algorithm for highway decision-making of connected and automated vehicles," *Chin. J. Mech. Eng.*, vol. 38, no. 1, pp. 1–14, Jan. 2025.

[23] M. Karimi, C. Roncoli, C. Alecsandru, and M. Papageorgiou, "Cooperative merging control via trajectory optimization in mixed vehicular traffic," *Transp. Res. C, Emerg. Technol.*, vol. 116, Jul. 2020, Art. no. 102663.

[24] B. M. Albaba and Y. Yildiz, "Modeling cyber-physical human systems via an interplay between reinforcement learning and game theory," *Annu. Rev. Control*, vol. 48, pp. 1–21, Jun. 2019.

[25] Y. T. Chow, J. Darbon, S. Osher, and W. Yin, "Algorithm for overcoming the curse of dimensionality for time-dependent non-convex Hamilton–Jacobi equations arising from optimal control and differential games problems," *J. Sci. Comput.*, vol. 73, nos. 2–3, pp. 617–643, Dec. 2017.

[26] M. Bui, M. Lu, R. Hojabr, M. Chen, and A. Shriraman, "Real-time Hamilton–Jacobi reachability analysis of autonomous system with an FPGA," in *Proc. IEEE/RSJ Int. Conf. Intell. Robots Syst. (IROS)*, Sep. 2021, pp. 1666–1673.

[27] B. R. Kiran et al., "Deep reinforcement learning for autonomous driving: A survey," *IEEE Trans. Intell. Transp. Syst.*, vol. 23, no. 6, pp. 4909–4926, Jun. 2022.

[28] Z. Zhu and H. Zhao, "A survey of deep RL and IL for autonomous driving policy learning," *IEEE Trans. Intell. Transp. Syst.*, vol. 23, no. 9, pp. 14043–14065, Sep. 2022.

[29] P. Nilsson and N. Ozay, "Synthesis of separable controlled invariant sets for modular local control design," in *Proc. Amer. Control Conf. (ACC)*, Jul. 2016, pp. 5656–5663.

[30] J. Usevitch and D. Panagou, "Adversarial resilience for sampled-data systems using control barrier function methods," in *Proc. Amer. Control Conf. (ACC)*, 2021, pp. 758–763.

[31] M. Chen, S. L. Herbert, M. S. Vashishtha, S. Bansal, and C. J. Tomlin, "Decomposition of reachable sets and tubes for a class of nonlinear systems," *IEEE Trans. Autom. Control*, vol. 63, no. 11, pp. 3675–3688, Nov. 2018.

[32] H. M. Wang, S. S. Avedisov, T. G. Molnár, A. H. Sakr, O. Altintas, and G. Orosz, "Conflict analysis for cooperative maneuvering with status and intent sharing via V2X communication," *IEEE Trans. Intell. Vehicles*, vol. 8, no. 2, pp. 1105–1118, Feb. 2023.

[33] H. M. Wang, S. S. Avedisov, O. Altintas, and G. Orosz, "Intent sharing in cooperative maneuvering: Theory and experimental evaluation," *IEEE Trans. Intell. Transp. Syst.*, vol. 25, no. 9, pp. 12450–12463, Sep. 2024.

[34] H. M. Wang, S. S. Avedisov, O. Altintas, and G. Orosz, "Multi-vehicle conflict management with status and intent sharing under time delays," *IEEE Trans. Intell. Vehicles*, vol. 8, no. 2, pp. 1624–1637, Feb. 2023.

[35] H. M. Wang, S. S. Avedisov, O. Altintas, and G. Orosz, "Negotiation in cooperative maneuvering using conflict analysis: Theory and experimental evaluation," in *Proc. IEEE Intell. Vehicles Symp. (IV)*, Jun. 2024, pp. 2297–2302.

[36] K. Deng, S. S. Avedisov, H. M. Wang, O. Altintas, and G. Orosz, "Negotiation protocol design for cooperative maneuvering of connected automated vehicles using conflict charts," in *Proc. IEEE Intell. Vehicles Symp. (IV)*, Jun. 2025, pp. 2019–2024.

[37] H. M. Wang, S. S. Avedisov, O. Altintas, and G. Orosz, "Experimental validation of intent sharing in cooperative maneuvering," in *Proc. IEEE Intell. Vehicles Symp. (IV)*, Jun. 2023, pp. 1–6.

[38] B. Lehmann, H.-J. Gunther, and L. Wolf, "A generic approach towards maneuver coordination for automated vehicles," in *Proc. 21st Int. Conf. Intell. Transp. Syst. (ITSC)*, Nov. 2018, pp. 3333–3339.

[39] R. van Hoek, J. Ploeg, and H. Nijmeijer, "Cooperative driving of automated vehicles using B-splines for trajectory planning," *IEEE Trans. Intell. Vehicles*, vol. 6, no. 3, pp. 594–604, Sep. 2021.

[40] S. Oh, Q. Chen, H. E. Tseng, G. Pandey, and G. Orosz, "Sharable clothoid-based continuous motion planning for connected automated vehicles," *IEEE Trans. Control Syst. Technol.*, vol. 33, no. 4, pp. 1372–1386, Jul. 2025.

[41] C. Jiang, H. Gan, I. Vörös, D. Takács, and G. Orosz, "Safety filter for lane-keeping control," in *Proc. 16th Int. Symp. Adv. Vehicle Control*, 2024, pp. 371–377.

[42] Y. E. Sahin, Z. Liu, K. Rutledge, D. Panagou, S. Z. Yong, and N. Ozay, "Intention-aware supervisory control with driving safety applications," in *Proc. IEEE Conf. Control Technol. Appl. (CCTA)*, Aug. 2019, pp. 1–8.

[43] H. M. Wang, S. S. Avedisov, O. Altintas, and G. Orosz, "Multi-vehicle conflict management with status and intent sharing," in *Proc. IEEE Intell. Vehicles Symp. (IV)*, Jun. 2022, pp. 1321–1326.

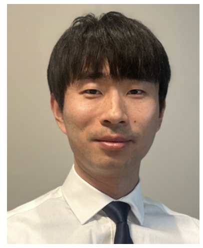

Hao M. Wang received the B.Eng. degree in mechanical and aerospace engineering from Nagoya University, Nagoya, Japan, in 2018, and the Ph.D. degree in mechanical engineering from the University of Michigan, Ann Arbor, USA, in 2024. He is currently an Engineer with Applied Intuition, Inc. His research interests include dynamics and control of connected and automated vehicles.

Sergei S. Avedisov (Member, IEEE) received the Ph.D. degree in mechanical engineering from the University of Michigan, Ann Arbor, USA, in 2019. He is currently with Toyota Motor North America Research and Development, InfoTech Laboratories, as a Cooperative Automated Driving Engineer. His research interests include cooperative automated driving, cooperative perception, cooperative maneuvering, vehicle-to-everything communications, and cooperative platooning in mixed traffic.

Onur Altintas received the Ph.D. degree in electronics engineering from The University of Tokyo. Since 1999, he has been with Toyota Group in various roles in New Jersey, Tokyo, and California. He is currently the Head and a Fellow with InfoTech Laboratories, Toyota Motor North America Research and Development. He has been the Co-Founder and the General Co-Chair of the IEEE Vehicular Networking Conference (IEEE VNC) since 2009. He serves as an Associate Editor for *IEEE Intelligent Transportation Systems Magazine*, *IEEE Vehicular Technology Magazine*, and IEEE TRANSACTIONS ON INTELLIGENT VEHICLES. He is an IEEE Vehicular Technology Society Distinguished Lecturer.

Gábor Orosz (Senior Member, IEEE) received the M.Sc. degree in engineering physics from Budapest University of Technology, Hungary, in 2002, and the Ph.D. degree in engineering mathematics from the University of Bristol, U.K., in 2006. He is currently a Professor of mechanical engineering and a Professor of civil and environmental engineering with the University of Michigan, Ann Arbor, USA. He is the leading author of the monograph 'Dynamics and Control of Connected Vehicles' published in 2025. His research interests include nonlinear dynamics and control, time delay systems, machine learning, and data-driven systems with applications to connected and automated vehicles, traffic flow, and biological networks.